A&A 440, 1133–1151 (2005)
DOI: 10.1051/0004-6361:20041774
© ESO 2005

Astronomy & Astrophysics

Bright OB stars in the Galaxy

II. Wind variability in O supergiants as traced by Hα

N. Markova[1], J. Puls[2], S. Scuderi[3], and H. Markov[1]

[1] Institute of Astronomy, Bulgarian National Astronomical Observatory, PO Box 136, 4700 Smoljan, Bulgaria
e-mail: nmarkova@libra.astro.bas.bg;rozhen@mbox.digsys.bg
[2] Universitäts-Sternwarte, Scheinerstrasse 1, 81679 München, Germany
e-mail: uh101aw@usm.uni-muenchen.de
[3] INAF – Osservatorio Astrofisico di Catania, Viale A. Doria 6, 95125 Catania, Italy
e-mail: scuderi@ct.astro.it

Received 2 August 2004 / Accepted 8 May 2005

Abstract. We investigate the line-profile variability (lpv) of Hα for a large sample of O-type supergiants (15 objects between O4 and O9.7), in an objective, statistically rigorous manner. We employed the Temporal Variance Spectrum (TVS) analysis, developed for the case of photospheric absorption lines and modified by us to take into account the effects of wind emission. By means of a comparative analysis we place constraints on the properties of this variability – quantified in terms of a mean and a newly defined fractional amplitude of deviations – as a function of stellar and wind parameters. The results of our analysis show that all the stars in the sample show evidence of *significant* lpv in Hα, mostly dominated by processes in the wind. The variations occur between zero and 0.3 v_∞ (i.e., below $\sim$1.5 $R_\star$), in good agreement with results from similar studies.

A comparison between the observations and corresponding line-profile simulations indicates that for stars with *intermediate* wind densities the properties of the Hα variability can be explained by simple models consisting of coherent or broken shells (blobs) uniformly distributed over the wind volume, with an intrinsic scatter in the maximum density contrast of about a factor of two. For stars at lower and higher wind densities, on the other hand, we found certain inconsistencies between the observations and our predictions, most importantly concerning the mean amplitude and the symmetry properties of the TVS. This disagreement might be explained by the presence of coherent large-scale structures, partly confined in a volume close to the star.

Interpreted in terms of a variable mass-loss rate, the observed variations of Hα indicate changes of $\pm$4% with respect to the mean value of $\dot{M}$ for stars with stronger winds and of $\pm$ 16% for stars with weaker winds. The effect of these variations on the corresponding wind momenta is rather insignificant (less than 0.16 dex), increasing only the local scatter without affecting the Wind Momentum Luminosity Relationship.

Key words. stars: early type – stars: mass-loss – stars: winds, outflows – methods: data analysis

1. Introduction

The basic philosophy underlying present-day hot star model atmospheres is the assumption of a globally stationary and spherically symmetric stellar wind with a smooth density stratification. Although these models are generally quite successful in describing the overall wind properties, there are theoretical considerations, supported by much observational evidence, that indicate that hot star winds are very far from being smooth and stationary.

The most common approach used to study wind variability in optical and UV domains is to follow line-profile variability (lpv) of one or several spectral lines, formed in different regions, in order to determine relevant time-scales and variability patterns and thus to obtain insight into the nature and the physical origin of the variations. This kind of survey requires long sets of stellar spectra with high S/N ratio and high temporal resolution, which implies that only few objects have been investigated so far. Through such investigations clear evidence for the presence of large-scale time-dependent wind perturbations (e.g., in the form of Discrete Absorption Components, DACs) was found in UV (Prinja et al. 1992; Massa et al. 1995; Prinja et al. 1996; Kaper et al. 1999; Prinja et al. 2002) and optical (Fullerton et al. 1992; Prinja & Fullerton 1994; Rauw et al. 2001; Prinja et al. 2001; Markova 2002) spectra of many O and early B stars. Since DACs have been observed in WR stars (Prinja & Smith 1992) and in an LBV (Markova 1986) as well, they are thought to be a fundamental property of radiative driven stellar winds.

Another source of lpv in hot stars winds is small-scale structures (clumps) which are believed to result from strong instabilities in the wind itself (Owocki et al. 1988; Feldmeier 1995; Owocki & Puls 1999). While the clumped nature of WR

Article published by EDP Sciences and available at http://www.edpsciences.org/aa or http://dx.doi.org/10.1051/0004-6361:20041774

winds was unambiguously proven by observations, the presence of clumps in O-star winds has so far relied on indirect evidence only (Crowther et al. 2002; Bianchi & Garcia 2002; Markova et al. 2004).

Wind structures and temporal variability are among the most important physical processes that may significantly modify the mass loss rates derived from observations. Since accurate mass loss rates are crucial for evolutionary studies (e.g., Meynet et al. 1994) and for extra-galactic distance determinations (via the Wind Momentum Luminosity Relationship (WLR), cf. Kudritzki & Puls 2000), it is particularly important to know to what extent the outcome of these studies might be influenced by uncertainties in $\dot{M}$ due to the effects of wind structures and variability. Indeed, Kudritzki (1999) has noted that wind variability is not expected to affect the concept of the WLR significantly. However, this suggestion is based on results obtained via a detailed investigation of one object alone, while similar data for a large number of stars of different spectral types and luminosity classes are needed to resolve the problem adequately.

Following the outlined reasoning, a project to study the effects of wind structure and variability in Galactic O-type stars has been recently started by our group. While in a previous paper (Markova et al. 2004, Paper I) we have dealt with problems concerning the WLR and the effects of wind clumping, in the present one we address the question of wind variability as traced by Hα and the dependence (if any) of the properties of this variability on fundamental stellar and wind parameters. In particular, in Sect. 2 we describe the observational material and its reduction. In Sect. 3 we outline the method used to detect and analyze the Hα lpv. In Sects. 4, 5 and 7 the results of our analysis are presented in detail while in Sect. 6 the outcomes of some simple 1- and 2-D simulations are described. In Sect. 8 we summarize the major results and give some comments and conclusions.

2. Observations and data reduction

Our sample consists of 15 Galactic supergiants with spectral classes from O4 to O9.7, all drawn from the list of stars analyzed by Markova et al. (2004) in terms of their mass-loss and wind momentum rates. Table 1 lists the objects along with some of their stellar and wind parameters, as used in the present study. All data are taken from Paper I.

A total of 82 high-quality Hα spectra ($R = 15\,000$) of the sample stars were collected between 1997 and 1999. The observations were obtained at the Coudé focus of the 2 m RCC telescope at the National Astronomical Observatory (Bulgaria) using an ELECTRON CCD (520×580, $22 \times 24\ \mu$) and a PHOTOMETRIC CCD (1024×1024, $24\ \mu$)[1]. For all stars but one the S/N ratio, averaged within each spectral time series, lies between 150 to 250, while in the case of HD 190429 it is ~100.

The temporal sampling of the data for each target is not systematic but random, with typical values of the minimum and maximum time intervals between successive spectra of 1 to 2 and 7 to 8 months, respectively. In several cases observations with a time-resolution of 1 to 5 days are also available, but in none of these cases do these observations dominate the corresponding time series. Thus, we expect the results of our survey to be sensitive to variations that occur on a time-scale that is significantly larger than the corresponding wind flow time (of the order of a few hours).

More information about the observational material and its reduction can be found in Markova & Valchev (2000) and in Paper I. In particular, to reduce the observations we have followed a standard procedure (developed in IDL) which includes bias subtraction, flat-fielding, cosmic ray hit removal, wavelength calibration, correction for heliocentric radial velocity, water vapor line removal and re-binning to a step size of 0.2 Å per pixel.

3. Methodology and measurements

Since we were going to study a large number of objects and since in many cases our observations were not systematic but with large temporal gaps in between, our ability to characterize the wind variability of individual targets is restricted, e.g., we are not able to determine time-scales and variability patterns. Moreover, to work effectively, we would need to employ a simple and fast method to detect and quantify lpv and to constrain the properties of this variability as a function of fundamental stellar and wind parameters of the sample stars.

Fullerton et al. (1996) have developed a very sensitive and rigorous method to determine lpv that is poorly sampled in time. This method, called Temporal Variance Spectrum (TVS) analysis, was proven to be a powerful tool to detect and compare lpv of pure absorption profiles. However, its use on profiles influenced by wind emission has not been tested systematically. Although the application of the TVS technique to detect lpv in emission lines does not seem to pose serious problems (e.g., Kaufer et al. 1996; Kaper et al. 1997; Markova 2002), its implication for the objectives of a comparative analysis (e.g. to compare the strength of lpv in different lines or different stars) needs to be carefully investigated.

To study the Hα variability of the stars in our sample we modified the TVS analysis in order to take into account the effect of wind emission.

To compute the *TVS* of Hα as a function of velocity across the line and to determine the velocity width over which *significant* variability occurs, ΔV, we followed Fullerton et al. (1996) but assumed that the noise is dominated by photon noise[2].

[1] The use of different detectors is not expected to bias the homogeneity of our sample because the noise characteristics of these two devices are practically the same. The root-mean-square (rms) read-out noise of the ELECTRON CCD is 3 electrons per pixel (i.e. 1.5 ADU with 2 electrons per ADU) while the rms read-out noise of the PHOTOMETRIC CCD is 3.3 electrons per pixel (2.7 ADU with 1.21 electrons per ADU).

[2] This assumption seems to be justified because we rely on Coudé spectra of relatively high quality.

Table 1. Stellar and wind parameters of the sample stars used in the present study. All data are taken from Markova et al. (2004).

Object	Sp	$v_{\rm sys}$	$T_{\rm eff}$	$R_\star$	$\log g$	$Y_{\rm He}$	$\log L$	$v \sin i$	v_∞	β
HD 190 429A	O4If+	−36	39 200	20.8	3.65	0.14	5.97	135	2400	0.95
HD 16 691	O4If	−51	39 200	19.8	3.65	0.10	5.92	140	2300	0.96
HD 14 947	O5If	−56	37 700	25.6	3.56	0.20	6.08	133	2300	0.98
HD 210 839	O6If	−71	36 200	23.0	3.48	0.10	5.91	214	2200	1.00
HD 192 639	O7Ib(f)	−7	34 700	17.2	3.39	0.20	5.59	110	2150	1.09
HD 17 603	O7.5Ib(f)	−40	34 000	25.2	3.35	0.12	5.88	110	1900	1.05
HD 24 912	O7.5I(f)	59	34 000	25.2	3.35	0.15	5.88	204	2400	0.78
HD 225 160	O8Ib(f)	−40	33 000	22.4	3.31	0.12	5.73	125	1600	0.85
HD 338 926	O8.5Ib	−9	32 500	22.7	3.27	0.12	5.72	80	2000	1.00
HD 210 809	O9Iab	−90	31 700	19.6	3.23	0.14	5.54	100	2100	0.91
HD 188 209	O9.5Iab	−16	31 000	19.6	3.19	0.12	5.51	87	1650	0.90
BD+56 739	O9.5Ib	−5	31 000	19.6	3.19	0.12	5.51	80	2000	0.85
HD 209 975	O9.5Ib	−18	31 000	19.2	3.19	0.10	5.49	90	2050	0.80
HD 218 915	O9.5Iab	−84	31 000	19.6	3.19	0.12	5.51	80	2000	0.95
HD 18 409	O9.7Ib	−51	30 600	15.7	3.17	0.14	5.29	110	1750	0.70

In this case, the *TVS* for the pixels in Col. j (i.e., at wavelength/velocity j) is calculated from

$$TVS_j = \sum_i^N \frac{w(i)(S_{ij} - \overline{S_j})^2}{S_{ij}(N-1)} \quad (1)$$

where $\overline{S_j}$ is the weighted mean spectrum for the jth pixel, averaged over a time series of N spectra, and given by

$$\overline{S_j} = \frac{\sum_i^N S_{ij} w_i}{N}, \quad (2)$$

with the weighting factors, w_i, given by

$$w_i = \left(\frac{\sigma_0}{\sigma_{ic}}\right)^2 \quad (3)$$

where

$$\sigma_0 = \left(\frac{1}{N}\sum_i^N \sigma_{ic}^{-2}\right)^{-1} \quad (4)$$

and σ_{ic} is the value of the noise in the i-th spectrum, averaged over a certain number of continuum pixels (40 in our case).

The rms deviations (rms = $TVS^{0.5}$) as a function of velocity across Hα for the time series of each target are shown in the top panels of Figs. 1 to 3. The level of deviations in the continuum, σ_0, is represented by a dashed line, while the threshold of *significant* lpv, fixed at the corresponding 99% confidence level of the $\sigma_0^2 \chi^2_{N-1}$ distribution, is marked with a dashed-dotted line. Although our implementation is in terms of $TVS^{0.5}$, hereafter we continue to refer to the "TVS" and the "TVS analysis", respectively[3].

To localize the Hα lpv in velocity space we used the "blue" and "red" velocity limits of *significant* variability, $v_{\rm b}$ and $v_{\rm r}$, introduced by Fullerton et al. (1996). The measurements have been performed interactively to fix the positions of the two points where the TVS crosses the horizontal line representing the threshold of *significant* lpv. The accuracy of these measurements depends on the quality of the data used and on the strength of the lpv. For example, in the limiting case of a strong lpv (i.e., a TVS with large amplitudes and steep spectral gradients) the accuracy of the individual measurements might be as good as ±20 km s^{-1} . Alternatively, in the case of a weak lpv (e.g., with amplitudes just above the threshold of *significant* variability) the determination of the velocity limits might become so uncertain that different positions of almost similar probability may exist for each limit. In these latter cases and in order to assess the effects of such uncertainties on the outcomes of our analysis, we provide two pairs of estimates for $v_{\rm b}$ and $v_{\rm r}$. These two sets of values, expressed in km s^{-1} , are listed in Col. 6 of Table 2 as the first and a second entry. We consider the first entry as the more reliable one and will refer to it as the "conservative case".

As a by-product of the measurement of $v_{\rm b}$ and $v_{\rm r}$, we obtain the total velocity width over which *significant* variability in Hα occurs, $\Delta V = (v_{\rm r} - v_{\rm b})$. In order to find some constraints on the distribution of the lpv in *physical* space, we furthermore determined the radial distance $r_{\rm max}$, where $v(r = r_{\rm max}) = v_{\rm b}$, assuming that the wind velocity obeys a standard law of the form

$$v(r) = v_\infty\left(1 - b\frac{R_\star}{r}\right)^\beta, \quad (5)$$

$$b = 1 - \left(\frac{v_{\rm min}}{v_\infty}\right)^{1/\beta}, \quad (6)$$

with β and v_∞ from Table 1 and $v_{\rm min} = 1.0$ km s^{-1} . The obtained estimates of $r_{\rm max}$, expressed in units of $R_\star$, are given in Col. 7 of Table 2. Emission variability is difficult to localize and could in principle be due to the net effect of fluctuations that occur in different locations under different conditions and therefore consider these estimates as upper limits only.

To quantify and compare lpv, Fullerton et al. (1996) have introduced two parameters, called mean and fractional

[3] Root mean square deviations have been used instead of the TVS itself since the former quantity scales linearly with the size of the deviations. Thus, it is more appropriate for a direct comparison of the strength of lpv in various stars (see also Fullerton et al.).

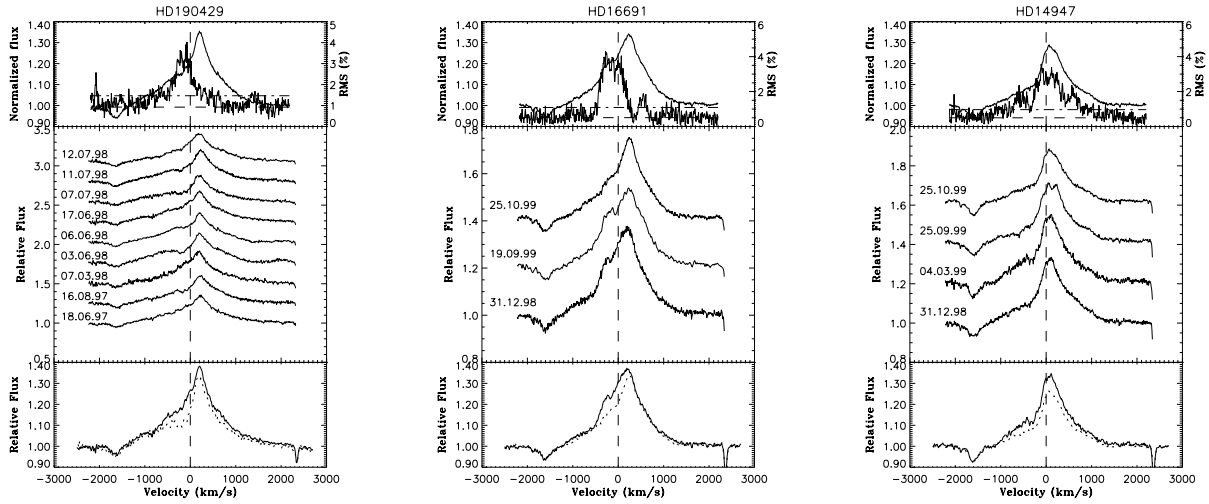

Fig. 1. Stars of early spectral type (O4/5). *Upper part of each panel*: mean Hα profiles (thick line) and rms deviations as a function of velocity across the line. *Middle part of each panel*: time-series of observed Hα profiles. *Lower part of each panel*: Hα profiles with maximum and minimum wind emission in the time series. Velocity scale centered at the corresponding systemic velocity.

amplitude of deviations, $A_{\rm lpv}$ and $a_{\rm lpv}$. In the following we will refer to these quantities as to $A_{\rm F}$ and $a_{\rm F}$ (with "F" referring to Fullerton). The first parameter is expressed in units of the normalized continuum flux, while the second one is a dimensionless quantity. The authors define these quantities as follows:

$$A_{\rm F} = \frac{1}{\Delta V}\int_{v_{\rm b}}^{v_{\rm r}} TVS_j^{0.5}\,{\rm d}v \tag{7}$$

$$a_{\rm F} = \frac{100\int_{v_{\rm b}}^{v_{\rm r}}\left(TVS_j-\sigma_0^2\right)^{0.5}\,{\rm d}v}{\int_{v_{\rm b}}^{v_{\rm r}}\left|\overline{S}_j-1\right|\,{\rm d}v}. \tag{8}$$

The above expressions imply the following. *First*, the mean amplitude of deviations is independent of profile type and thus can be used to evaluate the statistical significance of lpv both in absorption and in emission profiles. *Second*, the fractional amplitude depends (via the denominator) on the strength of the underlying spectral feature but does not differentiate between profiles in absorption and in emission. Particularly, it becomes a non-monotonic function of wind strength, with a maximum in those regions where the wind-emission has (more or less) completely filled in the photospheric absorption, i.e., where the net equivalent width within $[v_{\rm b}, v_{\rm r}]$ is close to zero. Therefore, this quantity is inappropriate to investigate profiles that are influenced by wind emission of different extents. This problem has already been outlined by Fullerton et al.

In order to optimize the fractional amplitude to account for the systematic difference in the strength of Hα as a function of wind strength, we decided to normalize the integral over the TVS to a quantity which we called "Fractional Emission Equivalent Width" (*FEEW*). With this new definition of the fractional amplitude, now denoted by $a_{\rm N}$ to distinguish it from Fullerton's parameter $a_{\rm F}$, this quantity is a measure of the *observed degree of variability per unit fractional wind emission*. "Fractional" refers here to the observed range of significant variability, $[v_{\rm b}, v_{\rm r}]$. Formally, $a_{\rm N}$ is given by[4]

$$a_{\rm N} = \frac{100\int_{v_{\rm b}}^{v_{\rm r}}\left(TVS_j-\sigma_0^2\right)^{0.5}\,{\rm d}v}{\int_{v_{\rm b}}^{v_{\rm r}}\left(\overline{S}_j-1\right)\,{\rm d}v-\int_{v_{\rm b}}^{v_{\rm r}}(S_j^{\rm phot}-1)\,{\rm d}v}. \tag{9}$$

The first term in the denominator of Eq. (9) represents the fractional equivalent width of the observed profile (positive for emission and negative for absorption), while the second one gives the fractional equivalent width of the photospheric component of Hα (always negative). In total, the denominator thus gives the fractional *wind* emission (always positive). A further discussion of $a_{\rm N}$ is given in Sect. 6.

The mean amplitude, as defined by Eq. (7), on the other hand, does not seem to pose any problem concerning an assessement of the statistical significance of variability across Hα. In their original study, Fullerton et al. noted that this quantity cannot serve as a comparative tool because it does not account for differences in the strength of the underlaying absorption feature. In contrast, in the case of Hα from O-type supergiants the mean amplitude might depend on the wind strength[5] and might therefore become of interest as well, in order to examine and to compare the wind variability in stars of various spectral types. Motivated by this possibility we redefined the mean amplitude to account (partially) for differences in the overall quality (i.e., in S/N) of the time series of the sample stars, by subtracting σ_0^2 from the TVS,

$$A_{\rm N} = \frac{100}{\Delta V}\int_{v_{\rm b}}^{v_{\rm r}}\left(TVS_j-\sigma_0^2\right)^{0.5}\,{\rm d}v. \tag{10}$$

The photospheric profiles of Hα required to derive the values of $a_{\rm N}$ have been selected from a grid of plane-parallel

[4] In this expression, we have accounted only for uncertainties caused by photon noise while the error due to small differences in the continuum level of individual spectra in a given time series is neglected.

[5] E.g., the numerator in Eq. (7) is expected to react to wind density (the higher the density the larger the emitting volume).

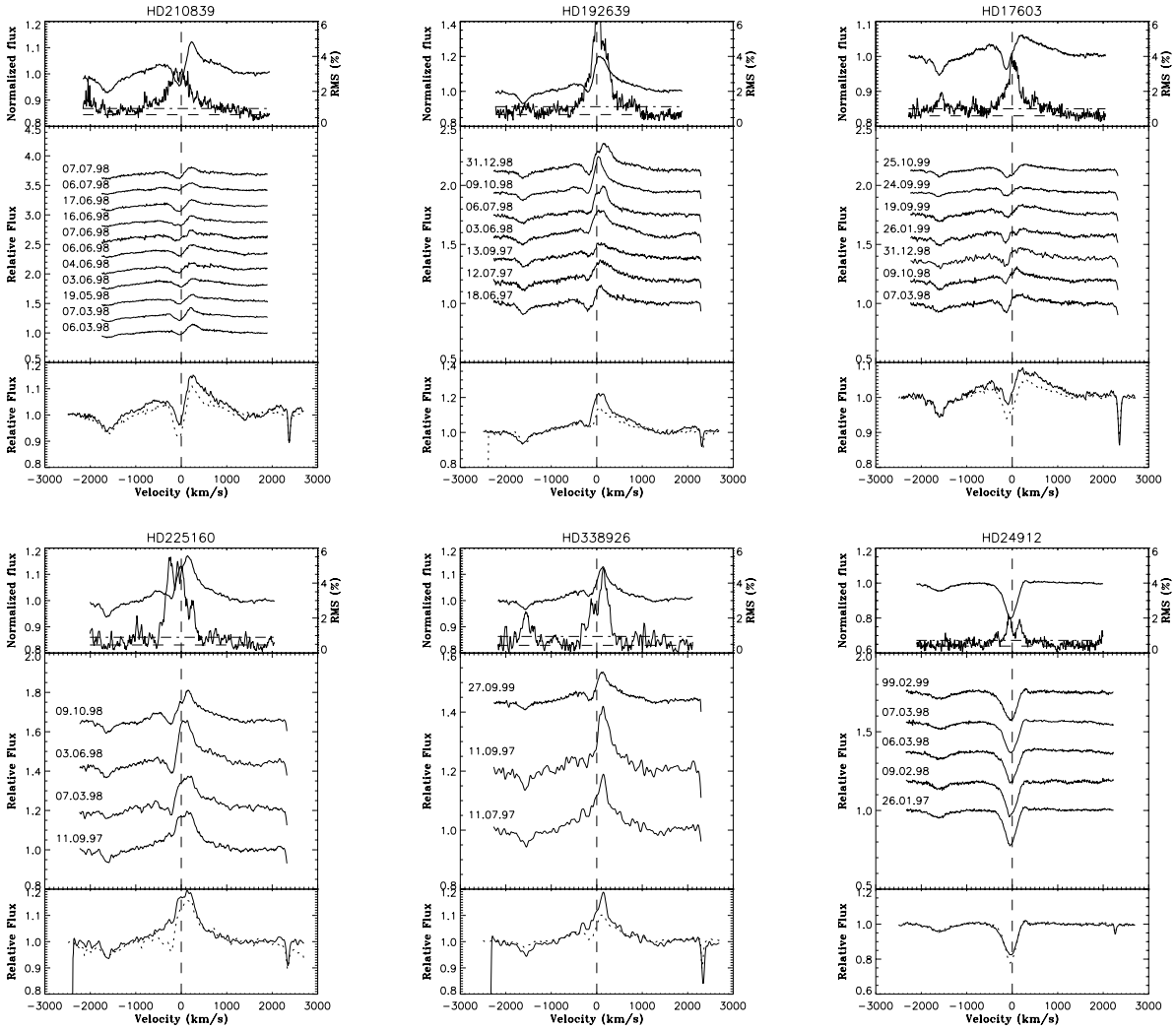

Fig. 2. As Fig. 1, but for stars of intermediate spectral type (O6 to O8.5).

models in dependence of the particular stellar parameters (Table 1; see also Paper I). Note that the (relative) uncertainty of the denominator becomes rather large in those cases where the wind-emission is only marginal, since in this case the errors introduced by uncertainties in the stellar parameters (affecting the actual choice of the photospheric profiles) become significant.

To estimate the uncertainty in $a_{\rm N}$ we followed Fullerton et al. (1996) but used a re-formulation (derived by A. Fullerton, priv. com.) of their Eq. (16). Additionally, we assumed that the errors in both σ_0 and *FEEW* are negligible and that the accuracy of the deviations for each pixel j within Hα is identical and equals σ_0[6]. Under these circumstances, standard error propagation gives:

$$\sigma(a_{\rm N}) = \sigma_0 \frac{100\,\Delta v}{FEEW}\left[\frac{1}{2(N-1)}\right]^{0.5}\left[\sum_j^n \frac{1}{\frac{TVS_j}{\sigma_0^2}-1}\right]^{0.5} \qquad (11)$$

where j runs over all the pixels between $v_{\rm b}$ and $v_{\rm r}$, while N and Δv denote the number of spectra in the time series and the discretized integration step, respectively. In our case $\Delta v \sim 9$ km s^{-1} (not to be confused with the total velocity width ΔV).

The factor of 100 appearing in Eqs. (8) to (11) converts the corresponding quantities to a percentage. The estimates of σ_0, $A_{\rm N}$ and $a_{\rm N} \pm \sigma(a_{\rm N})$) for each sample star are listed in Table 2, Cols. 5, 13 and 14, respectively.

To assess the contribution of changes in Hα line strength to the lpv detected by the TVS analysis, we estimated the mean value of the net wind emission, $\overline{W_{\rm em}}$, by subtracting the equivalent width (*EW*) of the photospheric profile, $W_{\rm phot}$, from the *EW* of the time-averaged observed profiles.

The observed equivalent widths were measured by integrating the line flux between limits which were set interactively, judging by eye the extension of the emission/absorption wings. These limits did not change for a given star but could vary for different stars. The internal precision of individual *EW* measurements, estimated in the way described in Markova & Valchev (2000), is better than 10%. The *EW* of the photospheric component was calculated by integrating over the appropriate synthetic profile. The $\overline{W_{\rm em}}$ estimates and their (standard) error are given in Col. 8 of Table 2, together with the *EW* of the photospheric components.

[6] The latter assumption is justified since we rely on Coudé spectra of relatively high signal to noise ratio.

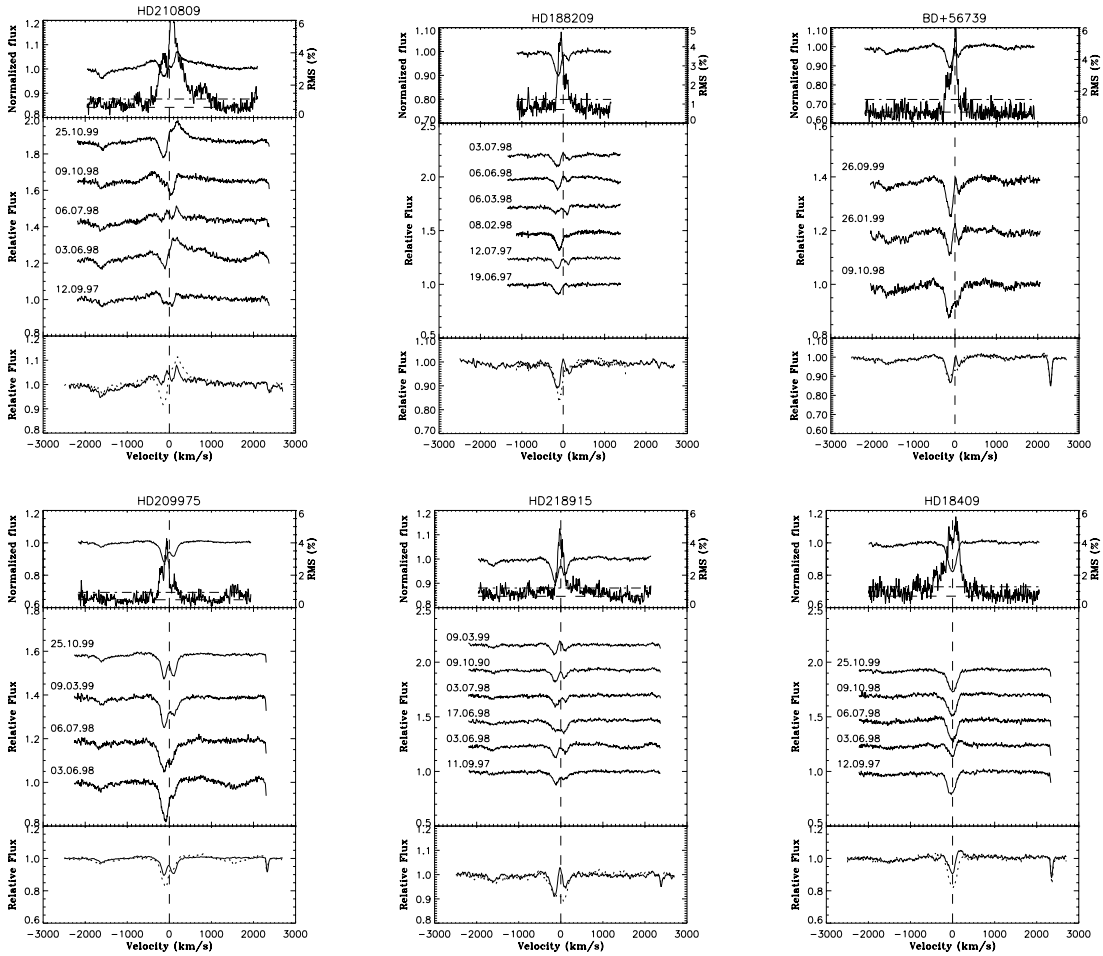

Fig. 3. As Figs. 1 and 2, but for stars of later spectral type (O9 to O9.7). Note the single-peaked, blue-shifted absorption profiles observed in HD 188 209 in June, 1997 and February, 1998. Profiles with similar shape have not been observed by Israelian et al. (2000) throughout their long-term monitoring campaign. Note also the P Cygni-like profile observed in HD 18 409 in June, 1998. This profile is completely different from the rest of the time series and indicates a strong increase in density in the innermost wind region.

Since in O-type supergiants Hα originates from processes taking place in the wind *and* in the photosphere, contributions from *absorption* lpv to the observed lpv might be expected (via the photospheric components of Hα and HeII λ6560). To investigate this possibility we consulted the literature (particular references are given below) concerning the presence of absorption lpv in our sample. In addition and as a secondary criterion, we used the TVS of the HeII λ6527 absorption line located at about 1650 km s^{-1} blue-wards of Hα. In those cases where the results of our TVS analysis of HeII λ6527 did not agree with the results from the literature, the latter were adopted[7].

To obtain constraints on the variability of mass-loss rates, for each star we determined lower and upper limits for $\dot{M}$. This has been done by fitting those Hα profiles that display the smallest and the largest wind emission present in the given time-series, by means of synthetic profiles. These have been calculated using stellar and wind parameters from Table 1 and employing the same method as used in Paper I. The accuracy of the $\dot{M}$ determinations is ±20% for stars with Hα in emission and ±30% for stars with Hα in absorption (Markova et al. 2004). The estimates of $\dot{M}_{\rm min}$ and $\dot{M}_{\rm max}$ as well as the amplitude of the $\dot{M}$ variability (given in percent of $\dot{M}_{\rm min}$) are listed in Cols. 9 to 11 of Table 2.

To quantify the wind strength we finally calculated the "mean wind density", $\langle\rho\rangle$, using data given in Table 1 and Table 2 (Col. 12), by means of

$$\langle\rho\rangle = \frac{\dot{M}}{4\pi(1.4R_\star)^2 v_\infty}, \qquad (12)$$

i.e., we considered the density at a typical location of 1.4 $R_\star$.

4. TVS analysis of Hα line-profile variability

4.1. Stars of early spectral types

Within our sample, the O4/5 supergiants HD 190 429A, HD 16 691 and HD 14 947 constitute the group with the highest effective temperature. Their Hα profiles, displayed in Fig. 1, appear to be completely in emission and consist of a well-developed emission core superimposed onto relatively strong

[7] Such inconsistencies may occur because the temporal sampling of our observations is not well-suited for studying lpv on the short time scales (e.g., hours) that seem to be typical for absorption lpv in O-type stars (Fullerton et al. 1996).

Table 2. Hα line profile and variability parameters. N denotes the number of available spectra. v_e is the velocity of the emission peak while v_b, v_r are the "blue" and "red" velocity limits of significant variability. All velocity data are measured with respect to the stellar rest frame and given in km s^{-1}. σ_0 is the standardized dispersion of the corresponding time-series. r_{max} (expressed in $R_\star$) denotes the upper limit in physical space where significant variations in Hα are present. $\overline{W_{em}}$ is the mean equivalent width of net wind emission and its standard deviation, both given in Å. W_{phot} is the equivalent width of the photospheric component. $\dot{M}_{min}$ and $\dot{M}_{max}$ (in 10^{-6} $M_\odot$ yr^{-1}) denote the corresponding limits if the observed variability is attributed to variations in $\dot{M}$ alone, while $\Delta\dot{M}$ is the amplitude of this variability expressed in percents of $\dot{M}_{min}$. $\langle\rho\rangle$ is the mean wind density (Eq. (12)), and A_N and a_N are the mean and the fractional amplitudes (Eqs. (10) and (9)), respectively.

Object	#	N	lpv(a)	v_e	σ_0*100.	$[v_b, v_r]$	r_{max}	$\overline{W_{em}}/W_{phot}$	$\dot{M}_{min}$	$\dot{M}_{max}$	$\Delta\dot{M}$	$\log\langle\rho\rangle$	A_N	a_N
HD 190 429	1	9	no	210	0.93	[−491, 234]	1.23	10.99 ± 0.63/3.23	13.0	14.0	8%	13.16	2.24	6.07 ± 0.03
						[−491, 363]							2.09	5.73 ± 0.03
HD 16 691	2	3	no	223	0.51	[−448, 266]	1.22	10.87 ± 0.81/3.23	12.0	13.0	8%	13.13	2.89	7.17 ± 0.02
HD 14 947	3	4	no	82	0.50	[−704, 747]	1.43	9.35 ± 0.90/3.24	14.5	16.0	10%	13.27	1.90	7.84 ± 0.02
HD 210 839	4	11	yes	220	0.67	[−633, 478]	1.40	4.74 ± 0.55/3.00	6.8	9.8	44%	13.42	1.92	11.63 ± 0.03
						[−838, 665]	1.61						1.73	12.95 ± 0.04
HD 192 639	5	7	no	140	0.67	[−393, 460]	1.27	6.15 ± 0.52/3.02	4.7	5.4	16%	13.38	3.36	13.77 ± 0.03
HD 17 603	6	7	yes	210	0.60	[−373, 619]	1.27	4.04 ± 0.49/2.84	5.5	7.2	31%	13.56	1.87	12.49 ± 0.05
HD 24 912	7	5	yes	−50	0.40	[−419, 309]	1.12	1.36 ± 0.14/2.85	4.5	5.2	16%	13.77	1.09	15.32 ± 0.14
HD 225 160	8	4	no	140	0.46	[−491, 384]	1.33	4.51 ± 1.04/2.62	5.1	5.7	12%	13.45	3.21	15.61 ± 0.02
HD 338 926	9	3	yes	140	0.44	[−352, 362]	1.21	4.54 ± 0.38/2.61	4.5	5.4	20%	13.59	2.48	11.78 ± 0.03
HD 210 809	10	5	no	10	0.63	[−336, 909]	1.15	3.63 ± 0.63/2.59	3.2	4.5	41%	13.60	2.77	24.11 ± 0.05
HD 188 209	11	6	yes	−6	0.72	[−176, 144]	1.09	1.56 ± 0.19/2.18	1.5	1.8	17%	13.87	2.67	16.37 ± 0.08
BD+56 739	12	3	no	13	0.69	[−295, 96]	1.12	1.78 ± 0.31/2.18	2.1	2.5	19%	13.80	2.84	24.66 ± 0.72
HD 209 975	13	4	no	26	0.48	[−277, 220]	1.09	1.36 ± 0.29/2.18	1.5	1.9	27%	13.92	1.90	20.85 ± 0.10
HD 218 915	14	6	no	−8	0.70	[−149, 206]	1.07	1.81 ± 0.24/2.18	1.6	2.0	25%	13.91	2.51	17.14 ± 0.10
HD 18 409	15	5	no	3	0.70	[−274, 268]	1.08	1.40 ± 0.47/2.17	1.5	2.2	47%	13.64	3.39	47.18 ± 0.11

and extended emission wings. The profiles are slightly asymmetric with a red wing being steeper than the blue one and a peak emission red-shifted with respect to the stellar rest frame.

For all stars, the mean amplitudes of deviations are significant at the 99% confidence level, indicating genuine lpv in Hα. Whereas for HD 190 429A and HD 16 691 the variations in Hα are distributed preferentially on the blue side of the emission peak, for HD 14 947 they extend almost symmetrically with respect to it. For HD 190 429A two values for v_r are provided, because of the rather small amplitudes of deviations at the red edge of the TVS.

Since the TVS analysis does not show evidence for *significant* lpv in HeII λ6527 (see upper panels of Fig. 1), we suggest that the variations observed in Hα are mostly (if not completely) due to processes in the wind. In the particular case of HD 190 429A, this assumption is supported by results reported by Fullerton et al. (1996), indicating that the photospheric CIVλ5801 line of this star does not show signatures of noticeable lpv.

Our measurements indicate that in each of the stars considered here the observed lpv in Hα has been accompanied by real (i.e., extending the measurement errors of 10%) variations in the equivalent width. In terms of the adopted model these variations in the Hα line strength can be reproduced by variations in $\dot{M}$ ranging from 8% (HD 190429A) to 10% (HD 14947).

4.2. Stars of intermediate spectral type

The subset of our supergiant sample with intermediate effective temperatures (32 000 K < T_{eff} < 37 000 K) includes six objects with spectral types ranging from O6 to O8.5. Apart from HD 24 912, whose Hα is in absorption and which will be considered separately at the end of this subsection, all the other objects exhibit Hα in emission (see Fig. 2).

The observations indicate the presence of noticeable Hα lpv in any star of this sub-group (see the middle parts of the panels in Fig. 2). The emission component varies from sharp, single-peaked emission to a double-peaked and somewhat broader structure, while the absorption component changes from a well-defined trough to a weak, hardly noticeable feature. At the same time, the morphology of the profiles does not change drastically and always consists of a P Cygni-like core on top of extended emission wings. The emission peak of the mean Hα profiles is red-shifted with respect to v_{sys}, whereas the position of the absorption dip is different for various stars and ranges from 260 to 360 km s^{-1} relative to the emission peak.

For the majority of the stars our TVS analysis reveals the presence of *significant* lpv concentrated at the P Cygni-like core. The variations are distributed almost symmetrically with respect to the rest wavelength. Only in HD 225 160 and in HD 338 926 they are concentrated towards the blue and the red side of the line, respectively. The velocity limits of *significant* variability are always well defined except for HD 210 839, where these limits seemed to be more uncertain.

To clarify the situation, we investigated the individual Hα profiles of the HD 210 839 time-series and found that part of the lpv detected between −900 and −500 km s^{-1} and between 500 and 700 km s^{-1} might be due to imperfect telluric line correction. This possibility was taken into account by providing two entries for v_b and v_r of HD 210 839 in Table 2.

Kaper et al. (1999) reported evidence for *significant* variability in Hα of HD 210 839 concentrated towards the blue side

of the line (between 0 and −400 km s^{-1}). The authors attributed this variability to the cyclic (P = 1.4 days) appearance of DACs in UV resonance lines. This finding is somewhat different from the one derived by us, where *significant* variability in Hα of HD 210 839 extends towards the emission peak of the line as well. This "inconsistency" might be explained by suggesting that in addition to the short-term variability caused by DACs there is another variability component that operates on a time scale longer than covered by the observations used by Kaper et al.

The morphology of Hα of HD 192 639 does not indicate any evidence for deviations from spherical symmetry and homogeneity, in contrast to the findings by Rauw et al. (2001). If not due to observational selection, this result might suggest that the wind structure observed by Rauw et al. (2001) was not a permanent but rather a transient feature of the wind, similar to the one observed in α Cam (Markova 2002).

Except for HD 17 603 and HD 338 926 no indication of *significant* absorption lpv was found. Regarding HD 210 839 and HD 192 639 this finding does not agree with results reported by Fullerton et al. (1996) and by de Jong et al. (1999)[8]. Thus, we conclude that, at least for four out of the five stars in this group, contributions from photospheric lpv can be expected.

For all stars a genuine variability in the equivalent width of Hα has been found. Neglecting the possible contribution from absorption lpv (if present) we found that the (rather extreme) variations in the Hα net wind emission can be accounted for by a 12% (HD 225 160) to 44% (HD 210 839) variation in $\dot{M}$.

HD 24 912 (ξ Per) was observed once in 1997, three times in 1998 and once in 1999. The Hα profiles (lower-right panel of Fig. 2) appear completely in absorption, in contrast to the profiles of the other sample stars of similar spectral type. The red wing is steeper than the blue one and the absorption dip is blue-shifted with respect to the stellar rest frame. Profiles with similar signatures are typical for stars with weaker winds where the Hα photospheric absorption is partly filled in by wind emission.

The TVS of Hα consists of a blue-shifted, single-peaked component plus a double-peaked structure with maximum amplitudes concentrated at the absorption core and at the red extension of the profile. In an absorption profile, a double-peaked TVS might indicate the presence of radial velocity variability caused by pulsations (Fullerton et al. 1996). Indeed, our measurements show that the velocity of the absorption core of Hα varies around a mean value of -43 ± 13 km s^{-1} [9]. Since the position of the absorption dip does not seem to depend on the line strength (i.e., on the strength of the wind emission) we suggest that the observed radial velocity variability is mostly (if not completely) due to changes in the stellar photosphere and probably caused by pulsations (de Jong et al. 1999, 2001).

In addition to this, another variability component seems to be present in HD 24 912, as indicated by the blue-shifted, single-peaked feature in the HαTVS, located between −200 and −450 km s^{-1} . This velocity interval is similar to the interval of the 2-d period variation established by Kaper et al. (1997) and by de Jong et al. (2001), and both findings might have the same origin.

The *EW* of Hα varies between 1.3 and 1.8 Å, in good agreement with the limits derived by Kaper et al. (1997). Interpreted as due to variations in the mean wind density, these limits comply with a ±16% variation in $\dot{M}$, which is smaller than the error of the individual $\dot{M}$ estimates (±25%, Markova et al. 2004) and thus insignificant. Again, this finding is consistent with corresponding results from Kaper et al. (1997). Based on simultaneous UV and optical observations of ξ Per, the latter authors suggested that the *EW* variability of Hα is caused by the presence of large-scale, time-dependent structures in the wind.

In summary, we conclude that the variability we have observed in ξ Per is a mixture of variations originating both from the photosphere (caused by non-radial pulsations) and from the wind (presumably connected to the appearance of DACs).

4.3. Stars of late spectral type

The subset of sample stars of late spectral type (O9 to O9.7, $T_{\rm eff}$ < 32 000 K) includes 6 objects. Five of them show Hα profiles with similar morphology whereas another one – HD 210 809 – exhibits a multitude of differently shaped Hα profiles and will be considered separately at the end of this subsection.

The Hα profiles of HD 188 209, BD+56 739, HD 209 975, HD 218 915 and HD 18 409 appear in absorption, partly filled in by wind emission (see Fig. 3). The shape of the profiles can vary, from star to star and for a given star as a function of time, from double-peaked absorption with a central reversal peaked at the stellar rest frame to an asymmetric, blue-shifted absorption feature, with the red wing being steeper than the blue one. Hα profiles with similar signatures have been found in early B-type supergiants as well, e.g., Ebbets (1982).

No indication of extended emission wings has been found in this subgroup, except for BD +56 739. This object shows weak, but clearly visible emission wings extending to about ±1200 km s^{-1} , suggesting a relatively strong wind[10].

All stars show evidence of real lpv in Hα. For part of the sample stars, the deviations are distributed almost symmetrically with respect to the stellar rest frame, with maximum amplitudes concentrated almost at the central reversal, whereas for others (e.g. HD 209 975), the variations are stronger blueward from the rest wavelength. In the particular case of HD 209 975 this blue-to-red asymmetry of the TVS might be explained by bluewards migrating DACs (Kaper et al. 1997). Two entries are given for HD 18 409, since the blue velocity limit for *significant* Hα variability is somewhat uncertain.

For none of the stars in this group have we found evidence of *significant* variability in the HeII λ6527 absorption line. This finding is consistent with the results reported by Fullerton et al. (1996) for the two stars in common, HD 188 209 and

[8] de Jong et al. (1999) have recognized HD 210 839 as a non-radial pulsator.

[9] The uncertainty in individual radial velocity measurements equals to ±4.5 km s^{-1} , i.e., half the bin step of 0.2 Å.

[10] Weak emission wings (±900 km s^{-1}) might be present also in HD 209 975.

HD 209 975. In contrast, Israelian et al. (2000) have reported evidence of quasi-periodic absorption lpv (with $P = 6.4^{\rm d}$) for HD 188 209. Since the data-set used by Israelian et al. (2000) is much more extended than the one used by us and by Fullerton et al. (1996), we consider their result as more reliable. Thus we assume that in five out of the six stars the observed variability in Hα is dominated by changes in the wind and that only in HD 188 209 a contribution from photospheric lpv is to be expected.

Our measurements show that the main source of lpv in Hα are changes in equivalent width. For all stars the $\dot{M}$ variations needed to account for the extreme changes detected in $\overline{W_{\rm em}}$ exceed the error of individual determinations and are therefore considered as real. As an example, for HD 188 209 we derived upper and lower limits of 1.5 and 1.75×10^{-6} $M_\odot$ per year, respectively, in full agreement with the estimates reported by Israelian et al. (2000).

HD 210 809. The individual spectra, shown in the middle part of the corresponding plot in Fig. 3, indicate the presence of dramatic lpv in Hα. The profiles change from a relatively weak absorption trough with a flat core via an ordinary/reverse P Cygni-like feature to a triple emission structure. In addition, strong emission wings extending to ~1500 km s^{-1} are clearly visible. Line profile variability with similar signatures has been discussed as an indication of long-lived, large-scale wind density perturbation(s), which co-rotate with the star, giving rise to additional line emission at various frequencies (Rauw et al. 2001, and references therein).

As might be expected from the observations, the distribution of lpv in Hα is asymmetric with respect to the rest wavelength, with maximum amplitudes concentrated at the P Cygni-like core. The smaller amplitude deviations located between 600 and 900 km s^{-1} are caused by the appearance of a bump on the red emission wing in the June 1998 line profile.

From the TVS of HeII λ6527, we found no indication of *significant* photospheric lpv, suggesting that the observed variations in Hα are caused by changes in the wind.

Although the observations give clear evidence for deviations from spherical symmetry, we applied our line-synthesis code (based on a spherical model) to find constraints on the mass-loss rate variability of the star. Fitting particularly the first and the last profile of the time series by model calculations, we found that the extreme variations in $\overline{W_{\rm em}}$ can be reproduced by variations of ±20% in $\dot{M}$.

5. Hα line-profile variability as a function of stellar and wind parameters

In order to obtain further clues concerning the origin of wind variability (as traced by Hα) in O supergiants, we examined various correlations between line profile parameters and parameters of the TVS of Hα, on the one hand, and fundamental stellar and wind parameters of the sample stars, on the other. To search for such correlations, we used the Spearman rank-order correlation test, described, for example, by Press et al. (1992). The main advantage of this test is that in addition to the correlation coefficient (more precisely, the linear correlation coefficient of ranks) it also calculates the statistical significance of this correlation (expressed as the two-sided significance of its deviation from zero), without any assumption concerning the distribution of uncertainties in the individual quantities.

5.1. Hα profile shape as a function of spectral type

An inspection of the *mean* Hα profiles of the sample stars (all supergiants), displayed in Figs. 1 to 3, shows that these profiles evolve as a function of spectral type from a slightly asymmetric emission with a peak value red-shifted with respect to $v_{\rm sys}$, via an emission feature with a P Cygni-like core, to a feature in absorption (with or without central emission reversal). In stars of early and intermediate spectral type extended emission wings can be seen, while in stars of late spectral type the presence of such wings is rare.

There are two stars that deviate from this behaviour, HD 24 912 and HD 210 809. The former one exhibits a pure absorption profile instead of a P Cygni-like profile (see Fig. 2). Consequently, its Hα line resembles much more those profiles from luminosity class III than from luminosity class I objects of the same spectral type. As we have already pointed out in Paper I, the parameters of HD 24 912 are somewhat insecure due to the uncertain distance – HD 24 912 is not a member of PerOB2 but a runaway star (Gies 1987). Thus it is rather likely that the discrepancy in profile shape is due to an erroneous (re-)assignment in luminosity class (Herrero et al. 1992) and suggest that the original value as assigned by Walborn (1973), luminosity class III, is more appropriate (see also Repolust et al. 2004).

The second outlier, HD 210 809, shows a P Cygni-like profile instead of an absorption profile partly filled in by wind emission. This is the only star in the sample for which our observations suggest a strong deviation from spherical symmetry. From the similarity to the Hα and HeII 4686 time-series of HD 192 639 observed and discussed by Rauw et al. (2001) (single and double peak structure in emission), we speculate that also here a "confined co-rotating wind" is present. This interpretation, if correct, would explain the "peculiar" shape of the mean Hα profile derived by us. Hereafter, we will refer to HD 24 912 and HD 210 809 as to "peculiar" stars.

The observed evolution of Hα in O-supergiants with spectral type (actually with $T_{\rm eff}$) is in fair agreement with results from theoretical line-profile computations performed in terms of NLTE, spherically symmetric, smooth stellar wind models, although the strength of the observed P Cygni-like core cannot be reproduced in most cases (e.g., Repolust et al. 2004)[11]. The main drivers of this evolution are: decreasing line emission caused by decreasing wind density (since $\dot{M}$ decreases with decreasing $T_{\rm eff}$ and $\log L/L_\odot$, see Vink et al. 2000) and decreasing contribution of the HeII λ6560 blend. (In contrast, purely photospheric Hα profiles of a given luminosity class do not change

[11] This problem has not been solved satisfactorily so far. In particular, it is still unclear if the blue-shifted absorption core is solely related to the HeII blend or other effects (clumps, deviations from 1-D geometry) have to be accounted for additionally.

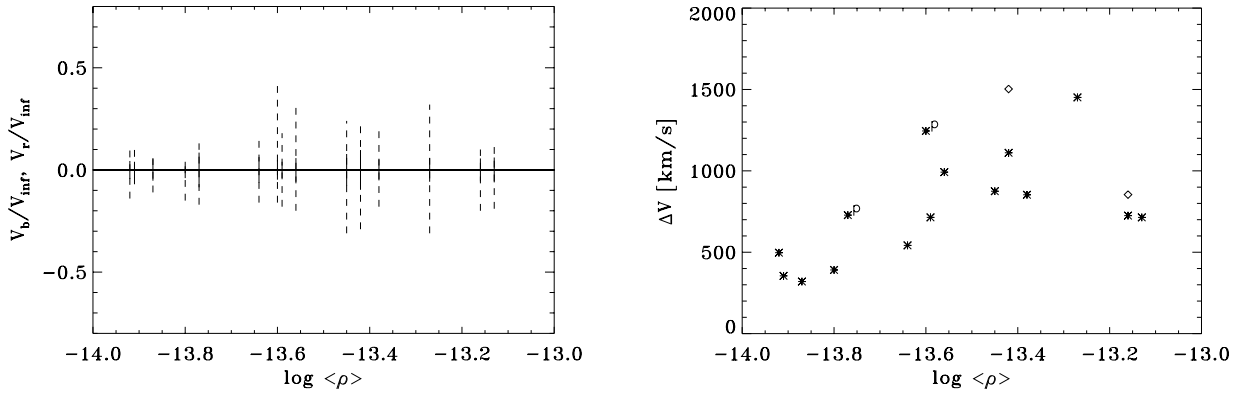

Fig. 4. Blue and red velocity limits (*left panel*) and velocity width (*right panel*) of *significant* lpv in Hα, as a function of mean wind density of the sample stars. Thick vertical lines denote the corresponding projected rotational velocity, $\pm v \sin i$. Asterisks refer to the conservative estimates for ΔV, while diamonds mark the non-conservative ones.

significantly as a function of $T_{\rm eff}$, because in this temperature regime the photospheric ionization fraction of neutral hydrogen remains fairly constant.) Outliers can occur either as a result of strong deviations from spherical symmetry and homogeneity in the wind (due to, e.g., fast rotation, CIRs, clumps) or as a result of an erroneous spectral type/luminosity class classification or uncertain/wrong parameters.

5.2. Red-shifted emission-peaks

Our observations suggest that the position of the emission peak of the Hαprofiles of O supergiants depends on the strength of the wind: for stars with weaker winds (Hα in absorption with/without central reversal) this peak is centered almost at the rest wavelength, whereas for stars with stronger winds (Hα in emission) it is red-shifted instead. This observation is supported by results of the correlation analysis, which shows that the velovity of the emission peak, $v_{\rm e}$ correlates significantly with $\langle\rho\rangle$, (.79/0.0007) and in addition with $T_{\rm eff}$ (.82/0.0003)[12].

Hereafter, numbers in brackets denote the Spearman rank correlation coefficient and the two-sided significance of its deviations from zero. Since the latter quantity measures the probability to derive a given correlation coefficient from uncorrelated data, smaller values mean higher significance of the correlation.

Red-shifted emission peaks have been observed in UV resonance lines of O-type stars, where this finding (in parallel with the presence of an extended absorption trough) can been explained in terms of "micro-turbulence" effects, with $v_{\rm micro}$ of the order of 0.1 v_∞ (e.g., Hamann 1980, and references therein; Groenewegen & Lamers 1989). On a first glance, the phenomenon seen in Hα seems to be somewhat similar. In contrast to the situation for UV resonance lines, however, our Hα profile simulations meet no problem in reproducing the red-shifted peak, even if the shift is large, *without any inclusion of micro-turbulence*. This can be seen clearly by comparing theoretical profiles with observations, e.g., Markova et al. (2004); Repolust et al. (2004). A closer inspection of the profile formation process reveals that the apparent shift of the emission peak results (at least in our simulations) from the interaction between the red-side of the Stark-broadened photospheric profile and the wind emission. Let us note that we do not exclude the presence of micro-turbulence but that we simply do not need it to reproduce the observed amount of $v_{\rm e}$.

[12] In this particular case and because of the reasons outlined above, the "peculiar" stars HD 210 809 and HD 24 912 have been discarded from the correlation analysis.

5.3. Properties of the TVS as a function of stellar and wind parameters

Before investigating the properties of the Hα TVS for our sample stars, let us point out that all results outlined below refer to the "conservative case" (see Sect. 3). Although the "non-conservative" data have not been analyzed in detail, they are included in the corresponding plots and we will comment on their influence on the final outcome.

5.3.1. Distribution of Hα line-profile variability in velocity space

In Fig. 4 we show the blue and red velocity limits (left panel, dashed) and the velocity width ΔV (absolute value, right panel) of Hα lpv as a function of the mean wind density. Thick vertical lines correspond to the projected rotational speed, $\pm v \sin i$. Asterisks refer to the conservative estimates for ΔV, while diamonds mark the non-conservative cases. In combination with the results described in Sect. 4, these figures indicate that:

i) for all stars the Hα lpv extends beyond the limits determined by stellar rotation and thus must be linked to the wind;
ii) in most of our sample stars the variations occur either symmetrically (within the error) with respect to the rest wavelength or with a weak blue-to-red asymmetry. For two objects, HD 17 603 and HD 210 809, the TVS has a noticeable red-to-blue asymmetry, while in other two stars, HD 190 429A and HD 16 691, the variations are stronger and more extended bluewards of the rest wavelength.
iii) the velocity width for *significant* variability in Hα is larger in stronger winds than in weaker ones. There are two stars

that deviate from this rule: HD 190 429A and HD 16 691 which exhibit variations over a velocity interval that is considerably smaller than expected from the strength of their winds.

Further analysis of the velocity data listed in Table 2 shows that in all sample stars *significant* lpv in Hα occurs below 0.3 v_∞ . Converted to physical space, this yields an upper limit of roughly 1.5 $R_\star$ for the observed variability. Additionally, we found a significant correlation between $r_{\rm max}$ and $\log\langle\rho\rangle$, (0.87/0.00001). This result as well as the possible dependence between ΔV and $\log\langle\rho\rangle$ (0.62 ± 0.01) are readily understood in terms of an increasing wind volume which contributes to the Hα emission, as a function of wind density.

Due to observational selection effects and other uncertainties affecting the determination of the velocity limits, the results described above might be questioned. However, note that: (i) the probability to obtain a symmetric TVS for a star with a strongly asymmetric wind, using snapshot observations, is very low; (ii) the established correlations between ΔV and $\log\langle\rho\rangle$ (right panel of Fig. 4) and between $r_{\rm max}$ and $\log\langle\rho\rangle$ are both physically reasonable, which in turn supports the reliability of the limits determined by us; (iii) although the limits and hence ΔV changes when non-conservative instead of conservative estimates are considered, the final outcome does not change (see Fig. 4 and Table 2).

Thus, we assume that the velocity limits determined here do not seem to be strongly biased by either observational selection or uncertainties in the measured quantities. (But see also the next sub-section.)

If a good temporal resolution of the variability time-scale is provided, the velocity distribution of lpv in Hα will allow us to obtain significant information about the wind geometry (Harries 2000). On the other hand, and as we shall show later on (see Sect. 6), even in the case of snapshot observations some hints about wind structures can be derived.

5.3.2. Mean and fractional amplitudes of deviations as a function of stellar and wind parameters

Our TVS analysis shows that the mean amplitude of deviations always exceeds the corresponding threshold for *significant* variability, indicating genuine variability in Hα. The actual values of $A_{\rm N}$ range between 1 and 4% of the continuum flux, without any clear evidence for dependence on stellar and wind parameters of the sample stars. This result is illustrated in the upper panel of Fig. 5, where the estimates for $A_{\rm N}$ are shown vs. $\log\langle\rho\rangle$.

This independence of $A_{\rm N}$ on $\log\langle\rho\rangle$ can have a twofold interpretation: first, *if* the mean amplitude is a reasonable measure for wind variability, then the wind variability is actually more or less independent on wind-strength. Second, the mean amplitude is not the appropriate tool to compare the strengths of Hα lpv.

Leaving aside these two possibilities, let us first consider the following problem. If we assume that the sources of observable variability are distributed over a certain volume which increases as a function of mean wind density (as it is suggested from the increase of $r_{\rm max}$ with $\log\langle\rho\rangle$), then one should expect that also A_N should increase with mean density, since the numerator of this quantity (the integral over $(TVS - \sigma_0^2)^{0.5}$) increases as a function of the emitting *volume*, whereas the denominator corresponds to an (increasing) 1-D quantity only. The fact that the *observed* mean amplitude is actually independent of $\log\langle\rho\rangle$ shows that such a simple model is not sufficient to explain the observations. We will come back to this point again in Sect. 6.

In contrast to the established independence of the mean amplitude on wind density, our analysis shows the presence of a *negative* correlation between the *fractional* amplitude of

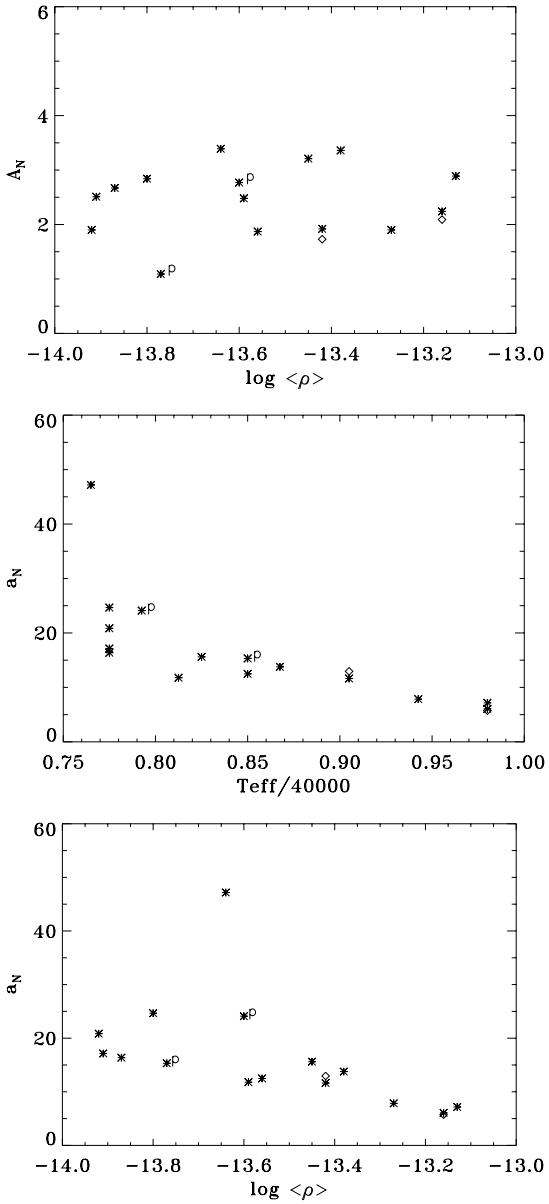

Fig. 5. Examples of significant correlations between the fractional amplitude of deviations, $a_{\rm N}$, as defined in the present study, and stellar and wind parameters of the sample stars. Distributions of the mean amplitude $A_{\rm N}$ are shown for comparison. Asterisks refer to the conservative estimates, while diamonds mark the non-conservative ones. Positions of the two "peculiar" stars are denoted by "P".

deviations, a_N, and a number of stellar/wind parameters. Scatter plots for the strongest correlations, with $T_{\rm eff}$ (0.92/0.000001) and with $\log\langle\rho\rangle$ (0.80/0.0003), are illustrated in Fig. 5. In particular, the decrease of a_N with increasing $\log\langle\rho\rangle$ suggests that the observed variability per unit fractional net emission is smaller in denser winds than in thinner ones.

The reliability of the derived values of the mean and fractional amplitudes has been checked in two ways: *first*, we examined the stability of the results against effects caused by observational selection and other uncertainties in the measured quantities; *second*, we checked the validity of the assumptions underlying our definitions of A_N and a_N.

In particular, to clarify to what extent these quantities (and again ΔV) might be influenced by observational selection effects, we proceeded as follows:

i) for the two stars with longest time series we reduced the number of spectra by about 30% while keeping the two most "extreme" profiles. The effect of this data manipulation on the TVS parameters was found to be insignificant;
ii) for the stars with longer time series ($N > 6$) we removed: (a) the spectrum with minimum Hα emission; (b) the spectrum with maximum Hαemission and (c) the two spectra with minimum and maximum wind emission and recalculated the TVS. In all the three cases the new estimates of σ_0 and ΔV turned out to be quite similar to the original ones: the established differences were less than a few percent. At the same time the TVS amplitudes changed by less than 10% for stars with Hα in emission and by about 15 to 20% for stars with Hα in (partly re-filled) absorption. The effect of these changes was again insignificant concerning the final results for ΔV, A_N and a_N.

The estimates of the TVS parameters are expected to depend strongly on the quality of the data used (i.e., on σ_0). To simulate higher S/N (about two times higher than the original values) we smoothed the spectra in each time series, using a boxcar average with a width of 4 pixels, and analyzed them in the same way as the original spectral series. Interestingly, while the effect of this data manipulation on the estimates of ΔV was surprisingly small (less than ±12% of the original values), the reaction of the TVS amplitudes turned out to be quite strong: both A_N and a_N, averaged over the whole sample, decreased by 37 and 33%, respectively, compared to their original values[13]. Most importantly, however, the new estimates of ΔV, A_N and a_N were found to obey similar dependences on $\log\langle\rho\rangle$ as implied by the original data set[14].

The derived independence of A_N on stellar and wind parameters as well as the negative correlations between these parameters and a_N cannot be explained in terms of either observational selection or uncertainties in the measured quantities.

[13] Part of this decrease might be due to the fact that the contribution of higher frequency variability (if any) has been reduced by smoothing.

[14] This result might no longer be true if large differences in the quality, i.e., in the standardized dispersion of the spectral time-series, σ_0, were present (the requirement of homogeneity).

6. Simulations of lpv in Hα

In order to account for the systematic difference in the strength of Hα as a function of spectral type/mean wind density, in Sect. 3 we optimized the fractional amplitude of deviations by normalizing the integral over the TVS to a quantity which we called fractional emission equivalent width, *FEEW* (see Eq. (9)).

The parameter a_N defined in this way is thus a measure for the observed variability (represented by the corresponding TVS) per unit fractional wind emission and has been used in the previous section to investigate the dependence of the observed variability on wind density. The results obtained might be interpreted as an indication that denser winds are less active than thinner winds, a finding which would give firm constraints on present hydrodynamical simulations.

Note, however, that (i) our definition of a_N implicitly assumes that the TVS amplitude is proportional to the corresponding amount of wind-emission and that (ii) this assumption has not been checked so far. In particular, if this assumption was justified, the derived values of a_N would provide a robust measure for the "observed" degree of wind-variability, as it is true for the *photospheric* lpv's described in terms of a_F.

6.1. 1-D model simulations

Thus, a test of our hypothesis is urgently required. Ideally, such a test would make use of at least 2-D models of instable winds, since the assumption of 1-D shells most probably overestimates the actual degree of variability.

Since 2-D simulations involving a consistent physical description are just at their beginning (Dessart & Owocki 2003) and since, to our knowledge, even for somewhat simpler multi-dimensional models no investigation concerning the dependence on wind parameters is available (Sect. 6.2), we have proceeded in the following way.

We have constructed a large number of very simple wind-models with variable Hα wind emission, in analogy to our stationary description (Paper I). The resulting profiles (10 per model) have been analyzed in the same way as the observed ones, i.e., by means of the TVS-analysis as described in Sect. 3. To allow for a direct comparison with results from our observations, we have added artificial Gaussian noise to the synthesized profiles ($S/N = 200$, which is a typical value), and have re-sampled the synthetic output onto constant wavelength bins corresponding to an average resolution of 15 000.

In order to account for the effects of wind disturbances of different size and density contrast in different geometries, we calculated various series of models: three consisting of spherical shells (series SS) and four consisting of broken shells (i.e., clumps, series BS1 and BS2). A summary of the various models and their designation is given in Table 3.

All simulations are based on our (quiet) model for HD 188 209 with $\dot{M} = 1.6\times 10^{-6}\ M_\odot\ {\rm yr}^{-1}$ (cf. Paper I). In order to investigate the reaction of the TVS of the synthetic profiles as a function of wind-strength we calculated, for each model series, 9 different models, with $\Delta \log \dot{M} \approx 0.1$, particularly

Table 3. Summary of simple 1-D simulations. Models denoted by"SS" refer to spherical shells, models denoted by "BS" to broken shells.

Series	Properties	max($\delta\rho/\rho_0$)
SS1	$\delta v = 0.5 v_{\rm th}$(H)	±0.7
SS2	$\delta v = 1.0 v_{\rm th}$(H)	±0.7
BS11	δm = const., Δp(core) = 0.1 $R_\star$	±0.35
BS12	δm = const., Δp(core) = 0.1 $R_\star$	±0.7
BS21	δm = const., Δp(core) = $R_\star$	±0.35
BS22	δm = const., Δp(core) = $R_\star$	±0.7
SS3	δm = const.	±0.35

at 0.8, 1.25, 1.6, 2.0, 2.5, 3.2, 4.0, 5.0 and 10.0×10^{-6} $M_\odot$ yr^{-1}. In this way, profile shapes varying from pure absorption via P Cygni type to pure emission have been obtained, covering all "observed" mean wind densities.

In all these models, only the density was allowed to be variable, whereas the velocity field and thus the NLTE departure coefficients (as a function of velocity) have been kept at their original value.

In a first step (series SS1/SS2), we used the most simplistic approach of disturbing the density, namely we varied this quantity in a random way as a function of radius only, i.e., we assumed spherical shells. This step, although rather unrealistic, was performed to check the stability of results from more "sophisticated" models (series BS1/BS2), which are described below.

The variations are defined in such a way as to allow for both positive and negative disturbances around the "quiet" model, in order to preserve the mean profile. We divided the wind into shells of equidistant velocity range, $\delta v_{\rm shell}$, where

$$\delta v_{\rm shell} = c \cdot v_{\rm th}({\rm H}), \quad c = 0.5, 1 \tag{13}$$

with $v_{\rm th}$(H) the thermal velocity of hydrogen. The different multipliers c define two different series, SS1 and SS2, respectively. Inside each of the shells, the density has been perturbed by a maximum amplitude of ±70%,

$$\rho = \rho_0(1 + \delta\rho/\rho_0), \quad \delta\rho/\rho_0 = -0.7 + 1.4 \cdot {\rm RAN}, \tag{14}$$

with ρ_0 the stationary density and RAN a random number uniformly drawn from the interval [0, 1]. The specific maximum amplitudes (for series SS, but also for series BS, see below) have been chosen in such a way that the resulting TVS-integrals and *FEEW*s are (roughly) consistent with the observed values. Lower maximum amplitudes would result in a too low degree of variability, and higher ones in too large values.

Note that the density contrast has been assumed to be constant within each of the shells, i.e., the number of drawn variables is given by the total number of shells, which is of the order of 80 for $v_\infty = 1650$ km s^{-1} and $c = 1$. Note also that only the wind has been allowed to be variable, i.e., we considered perturbations only outside the sonic point, located roughly at 20 km s^{-1} .

In this way, different and random amplitudes within the maximum range $\delta\rho/\rho_0 \in [-0.7, 0.7]$ are created for each individual shell. To allow for a temporal variability of the resulting profiles at "random" observation times (remember that our observations are typically separated by much more that one wind flow time) we performed, for each model, 10 simulations with different initialization of RAN and different locations of the contributing shells. The resulting 10 different profiles have been analyzed subsequently by means of the TVS method (an example is given in Fig. 6).

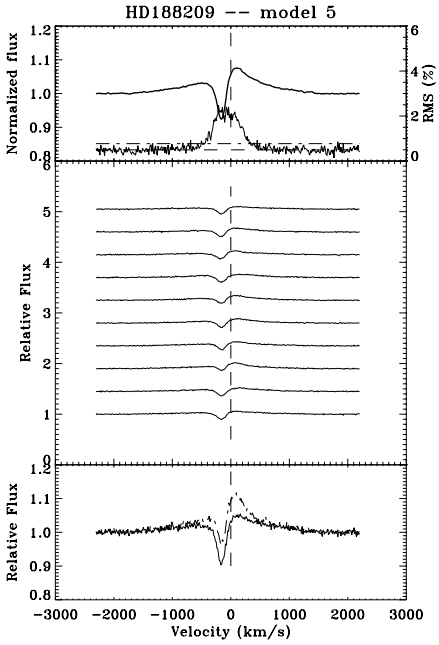

Fig. 6. As Fig. 1, but for *synthetic* profiles corresponding to model BS11 (broken shells, low amplitude) of HD 188 209, at $\dot{M} = 2.5 \times 10^{-6}$ $M_\odot$ yr^{-1} (see text).

Model series SS suffers from (at least) two major problems. At first, the assumption of *spherical* shells might amplify the lpv at all frequencies, since, especially in the wind lobes, there is only a weak chance that fluctuations will cancel out due to statistical effects. Second, our simulations define equal amplitudes of disturbance inside shells of equidistant range in *velocity* space. Accounting for the rather steep increase in velocity inside and the flat velocity field outside, this means that the contributing volume per shell is strongly increasing with radius, which might give too much weight to disturbances in the outer wind.

To solve both problems, we have calculated four additional model series, which should be more realistic than the above ones. At first, the spherical symmetry is broken by the following modification[15]. For the core-rays, we assume *coherent* shells (blobs), either of a relatively small lateral extent, $\Delta p \approx R_\star/10$ (series BS1) or of a larger extent, $\Delta p = R_\star$ (series BS2). For each of the non-core rays (distributed roughly logarithmically), on the other hand, we assume different locations of the density variations *per ray*, to simulate the presence of *broken* shells. The latter modification results in a lower TVS particularly in the red part of the profiles, due to cancellation

[15] Remember that the radiative transfer is performed in the usual $p-z$ geometry, with impact parameter p and height over equator z. The so-called *core rays* are defined by $p \le R_\star$, and the *non-core* rays passing *both* hemispheres of the wind lobes by $p > R_\star$.

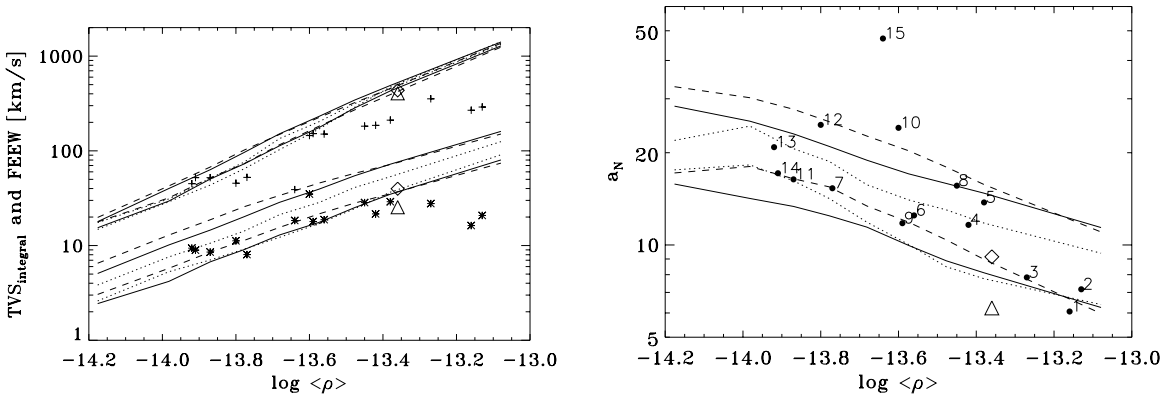

Fig. 7. *Left panel*: "observed" values of the numerator entering a_N ($TVS_{integral}$, asterisks) and of the fractional emission equivalent width (denominator of a_N, crosses), compared with simulated quantities, as a function of mean wind density $\log\langle\rho\rangle$. The dotted curves correspond to the simulations with spherical shells and constant δv spacing (SS1/SS2), and the other curves to the somewhat more realistic simulations accounting for broken shells and constant δm, BS11/BS12 (fully drawn) and BS21/BS22 (dashed). Note that inside each series of simulations the maximum amplitude of density-fluctuations, $\delta\rho/\rho_0$, is identical, i.e., independent on wind density. *Right panel*: as left, but for the fractional amplitude a_N (in %). The object numbers correspond to the entries given in Table 2. In both panels, the special symbols correspond to the data resulting from our TVS-analysis of the 3-D models presented by Harries (2000), cf. Sect. 6.2 (diamonds: spiral structure; triangles: clumpy structure).

effects. Note that we have convinced ourselves that different distributions of non-core rays gave very similar results.

In order to avoid the volume effect, instead of assuming $\delta\rho/\rho_0$ as random, however constant per shell of thickness δv = const., we now require that the random perturbations should occur in shells of *equal mass*,

$$\delta m_{\rm shell} = 4\pi r^2 \rho {\rm d}r, \tag{15}$$

with roughly 50 (broken) shells per model. Inside each broken δm shell, the density fluctuations are evaluated as above. For each of our simulations BS1 and BS2, we have used two different values for the maximum amplitude, $\max(\delta\rho/\rho_0) = \pm 0.35$ and ± 0.7 (BS11/BS21 and BS12/BS22, respectively), which gives a fair consistency with the range of observed variability.

Although the assumptions inherent to the various model series (SS vs. BS) are rather different, the results with respect to interesting quantities are fairly similar. The only difference concerns the distribution of the variability over the profile. For the spherical shells models, we find significant variability on the red side, whereas for the broken shell model the variability extends to larger blue velocities, due to the increased influence of the shells in front of the disk (cancellation effects in the lobes, see Fig. 6).

In Fig. 7 we now compare the outcome of all our simulations with the observations ("conservative" values). On the left panel, we have plotted the numerator entering a_N (lower set of curves), and the fractional emission equivalent width (*FEEW*, denominator of a_N, upper set of curves) as a function of mean wind density $\langle\rho\rangle$. Obviously, series SS and BS give similar results, as already noted. In particular, the results of models SS1 and models BS11 (lower dotted and fully drawn curves) are almost identical, which shows that a large number (~160) of spherical shells (model SS1) can simulate the outcome of a model with a lower number (~50) of broken shells and a lower density contrast. Moreover, it seems that the "volume effect" discussed above is insignificant, simply because Hα forms in the lower wind region. This similarity in the results points to a rather large probability that our results are robust and independent of the specific assumptions.

Interestingly, both the observations (except for the two objects with highest wind-density and *more localized TVS*, HD 190 429A and HD 16 691) and all simulations roughly follow a power-law for both quantities,

$$\log(TVS_{\rm integral}) \approx a + b\log\langle\rho\rangle$$
$$\log(FEEW) \approx c + d\log\langle\rho\rangle,$$

which immediately shows that our hypothesis of both quantities being proportional to each other fails. Note at first that the logarithmic dependence of the *FEEW* on $\log\langle\rho\rangle$ can be readily understood if one remembers that the *total* emission equivalent width of Hα scales as a power-law of mean wind-density (cf. Puls et al. 1996), and that the integration range $[v_{\rm b}, v_{\rm r}]$, entering the fractional equivalent width, is only weakly increasing with $\langle\rho\rangle$, if scaled to v_∞ and evaluated on a logarithmic scale (see Fig. 4). Since the TVS and its integral, on the other side, is also related to the mean wind-density (at least if the disturbances do not totally decouple from this quantity), the power-law dependence of this quantity on $\langle\rho\rangle$ can also be understood. The different and lower slope can be attributed to optical depth effects and the cancellation of fluctuations in the emission lobes (vs. the contributions from core-rays), at least in our simulations (where we "know" the origin of the variability). In total then, a_N becomes a decreasing function of $\log\langle\rho\rangle$,

$$\log a_N \approx (a-c) + (b-d)\log\langle\rho\rangle, \qquad b < d, \tag{16}$$

and since all our model series predict the same dependency, it is rather likely that this effect should be present also in more realistic simulations. In conclusion, we predict that a_N becomes a decreasing function of mean wind density, *even if the disturbances* (more precisely, their relative amplitudes) *are independent of* $\langle\rho\rangle$. The vertical off-set of this relation, on the other hand, depends strongly on the density contrast, i.e., on

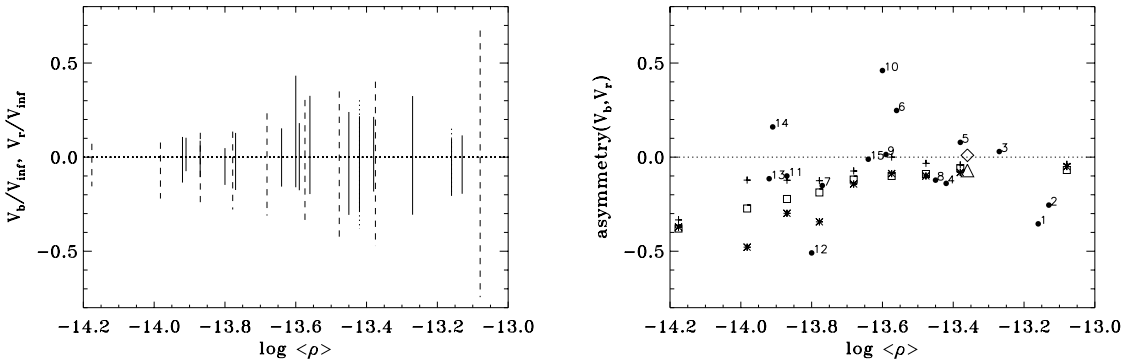

Fig. 8. *Left panel*: observed blue and red velocity limits, v_b, v_r (conservative and non-conservative values) in units of v_∞ , as a function of mean wind-density, compared with results from simulation BS21 (dashed). *Right panel*: observed asymmetry, $(v_r - |v_b|)/(v_r + |v_b|)$ (conservative values, black dots), compared with simulations (asterisks: BS21, squares: BS11, crosses: SS3). The object numbers correspond to the entries given in Table 2. The diamond and triangle refer to the data resulting from our TVS-analysis of the 3-D spiral and clumpy model presented by Harries (2000), cf. Sect. 6.2.

$\max(\delta\rho/\rho_0)$. These simulations, of course, refer to the case of fluctuations which are "globally" present, and will not explain effects from localized macro-structures such as CIRs.

The actual and predicted behaviour of a_N is shown in Fig. 7, right panel. For lower wind densities, the slopes of the relations for numerator and denominator are rather similar (optically thin winds, wind emission dominated by core-rays), so that the predicted amplitude a_N remains roughly constant or is even increasing, whereas from $\log\langle\rho\rangle \approx -14.0$ the predicted decrease is obvious. By comparison with observations, we find that almost all stars lie within the range suggested by BS11/BS12 and BS21/BS22, i.e., correspond to differences in (relative) amplitude within a factor of two. There are only two outliers, HD 210 809 (#10) and particularly HD 18 409 (#15, at $a_N \approx 50$). Remember that the former star has been designated as a "peculiar" object in Sect. 5.1, whereas the strong deviation of HD 18 409 is more likely due to uncertainties in wind parameters (Repolust et al. 2004): the large value of a_N is *not* due to a large TVS-integral, but due to a rather small value of its *FEEW* (located at $\log\langle\rho\rangle \approx -13.64$ and *FEEW* = 39 km s^{-1} in the left panel.

Even for the two objects with the largest wind densities, which have been found not to follow the individual relations for the TVS-integral and the *FEEW* (due to their rather localized variability), the results for a_N are consistent with the predictions. In our interpretation, this would mean that both stars have the same degree of activity as the other stars, only in different and more localized regions.

In summary, there are no indications of a dependence of wind activity on wind density, at least on basis of our present simulations; in our interpretation, the decrease of a_N is an artefact of the normalization, which (unfortunately) does not follow the same slope as the TVS-integral.

Furthermore, from our simulations, we may also conclude that the underlying disturbances (at given wind density) may introduce a scatter up to a factor of two in the maximum amplitude. Of course, more realistic simulations are needed before a final statement concerning this point can be given.

Further insight into the origin of the variability might be found from a comparison of observed vs. predicted velocity limits, v_b, v_r and particularly of their asymmetry, cf. Fig. 8. In the left panel of this figure, we compare these velocity limits (normalized to v_∞ , to obtain a unique scale) with our predictions, here with results from BS21 (broken shells, low amplitude). Obviously, for stars with low and intermediate wind strength ($[\log\langle\rho\rangle] < -13.2$) and except for HD 210 809 (at $\log\langle\rho\rangle = -13.6$, with strongly asymmetric velocity limits), our models do fairly reproduce the observed amount of increase of ΔV as a function of $\langle\rho\rangle$. Since at largest wind densities we have only two objects in our sample, it is not clear at present whether their discrepant behaviour is peculiar or not. Thus, except for the outliers, it might be concluded that the observed variability results from effects which are present *everywhere in the wind*, in accordance with our models. This conclusion seems to be also supported by the fact that HD 210 809 deviates from our predictions: for this star our observations have suggested the presence of large-scale wind disturbances which are localized rather than uniformly distributed over the wind volume.

The right panel of Fig. 8, however, shows also the shortcomings of our models. Plotted is the asymmetry of v_b, v_r by means of the expression $(v_r - |v_b|)/(v_r + |v_b|)$ (negative values correspond to blue-to-red, positive values to red-to-blue asymmetries, respectively). Let us first discuss the "theoretical" predictions. We have plotted the results for model series BS21 (asterisks), BS11 (squares) and for a model which has been constructed additionally for this comparison, namely a model with *spherical* shells and δm = const. (SS3, crosses). All three models have the same maximum amplitude, $\max(\delta\rho/\rho_0) = \pm 0.35$. Not surprisingly, the last model shows the least asymmetry, whereas model BS21 shows the largest one, due to the large lateral extent of the assumed broken shells in front of the stellar disk. Note that most models show a blue-to-red asymmetry, even those with spherical shells, whereas *in no case is a redwards asymmetry found*. This predicition, of course, results from cancellation effects in the lobes, compared to the situation for core-rays. For high wind-densities, all models converge to small or even negligible asymmetry, because of the increasing influence of the lobes. For model SS3 (spherical shells), symmetry is reached earliest, roughly at $\log\langle\rho\rangle = -13.5$.

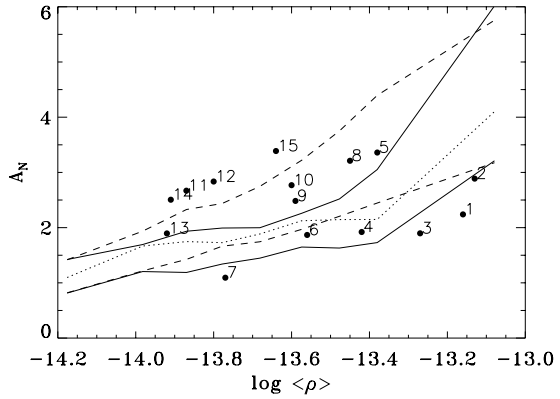

Fig. 9. "Observed" values of the mean amplitude of deviations, A_N (conservative values) compared with simulated quantities, as a function of mean wind density $\log\langle\rho\rangle$. The bold curves correspond to series BS11/BS12, the dashed curves to series BS21/BS22 and the dotted curve to series SS3 (spherical shells, low amplitude), respectively. Each series shows a positive correlation with mean wind density. The object numbers correspond to the entries given in Table 2.

With respect to the observations, the situation is as follows. At low and intermediate wind densities, only four objects display a *significant* asymmetry, mostly to the red, where the highest degree is found for HD 210 809 (#10, see above). The majority of stars, however, show either a small degree of asymmetry (both to the blue *and* to the red) or behave symmetrically. The predictions of series SS3 are closest to this behaviour. A symmetric TVS at low wind densities can be alternatively explained by models with co-rotating structures (e.g., CIRs), as will be discussed later on. For the two stars with larger wind densities, the predictions definitely deviate from what has been observed.

In Sect. 5.3.2 the mean amplitude of deviations, A_N, seems to be uncorrelated with mean wind density, at least for our sample. We speculated that if the sources of wind variability were (uniformly) distributed over the contributing wind volume, one should see a positive correlation. By means of our simple models, we can check this conjecture now and may find additional constraints on the origin of wind variability.

Figure 9 shows the behaviour of the simulated mean amplitude as a function of mean wind density, for series BS11/BS12, series BS21/BS22 and SS3, respectively. Actually, A_N *is* strongly correlated with $\langle\rho\rangle$, where the vertical offset is a function of (relative) amplitude $\delta\rho/\rho_0$. At a first glance, we might conclude that the observed values are again (i.e., as we have found for a_N) consistent with the models, if we allow for a variation in amplitude of roughly a factor of two.

A closer inspection, on the other hand, reveals that at least for two low density objects (HD 188 209, #11 and HD 218 915, #14) there is the following problem. The mean amplitudes of these objects are consistent with our simulations with larger $\delta\rho/\rho_0$ (BS22). Concerning the fractional amplitudes, a_N, however, they are consistent with our simulations for lower $\delta\rho/\rho_0$ (BS21, cf. Fig. 7), which in turn produce a much too large bluewards asymmetry in the TVS (Fig. 8). Remarkably, one of these objects (HD 218 915, #14) even suffers from an observed red-to-blue asymmetry.

Thus, from the comparison of mean amplitudes and asymmetry in the velocity limits we find a number of indications that at least two (from 3) low and the high density objects *cannot* be explained by our simple models consisting of *density fluctuations distributed everywhere in the wind*. If we return to our original TVS analysis (Figs. 3 and 1), the primary sources for these inconsistency can be clearly identified: (i) the strong variability of a central reversal at zero rest velocity, which gives rise to a rather large TVS within a narrow, symmetric velocity range for stars of weaker winds and (ii) the rather small extent of the observed variability, preferentially bluewards of the emission peak for stars of stronger winds.

In our models, a large variation at rest wavelength cannot be reproduced, at least if we allow for fluctuations of both positive and negative amplitude. Such a behaviour might be explained by radially extended, coherent structures in front of the disk, which would mimic a certain global increase of mass-loss by bringing the innermost part of Hα into emission. That our models can never reproduce a (strongly) localized variability has been discussed above.

6.2. 3D model simulations

Recently, Harries (2000) published results for 3-D line-profile simulations of Hα for ζ Pup, performed by means of his Monte Carlo stellar wind radiative transfer code. Two distinct models for the wind morphology have been considered: one with a co-rotating (one-armed) spiral structure and another one consisting of a clumpy wind. In the first case the author examined the effect of one spiral streamline of enhanced density on Hα, while in the latter one he considered random blobs propagating throughout the wind.

In order to obtain an impression as to what extent the outcome of our model analysis might be influenced by the fact that we consider 1-D instead of more realistic 3-D models, we analyzed the two different sets of synthetic profiles derived by Harries (kindly made available to us by the author), in the same way as for the time-series of our sample stars and for our own simulations. The corresponding results are shown in Fig. 10.

Apart from the impressive sequence of synthetic profiles which allows to easily follow any evolution of wind structure in time, a number of interesting features is noticeable.

In the first place, the distributions of amplitudes for the two models are rather different: in the one-armed spiral model, the derived TVS is double-peaked and *symmetric with respect to the stellar rest frame*, while in the clumped model it is single peaked with maximum amplitudes concentrated on the blue. In addition, for the clumped model the velocity range of *significant* variability shows a clear blue-to-red asymmetry ($v_b = -1670$, $v_r = 1440$ km s^{-1}) while for the spiral model it is almost symmetrical with respect to the rest wavelength ($v_b = -2010$, $v_r = 2050$ km s^{-1}).

Interestingly, also the parameters derived from the TVS analysis of the spectra for the 3-D clumped model are quite similar to the ones we have derived in terms of our 1-D broken shell (i.e., clumpy) models (see Figs. 7 and 8), whereas the small differences might explained by the fact that the spectra

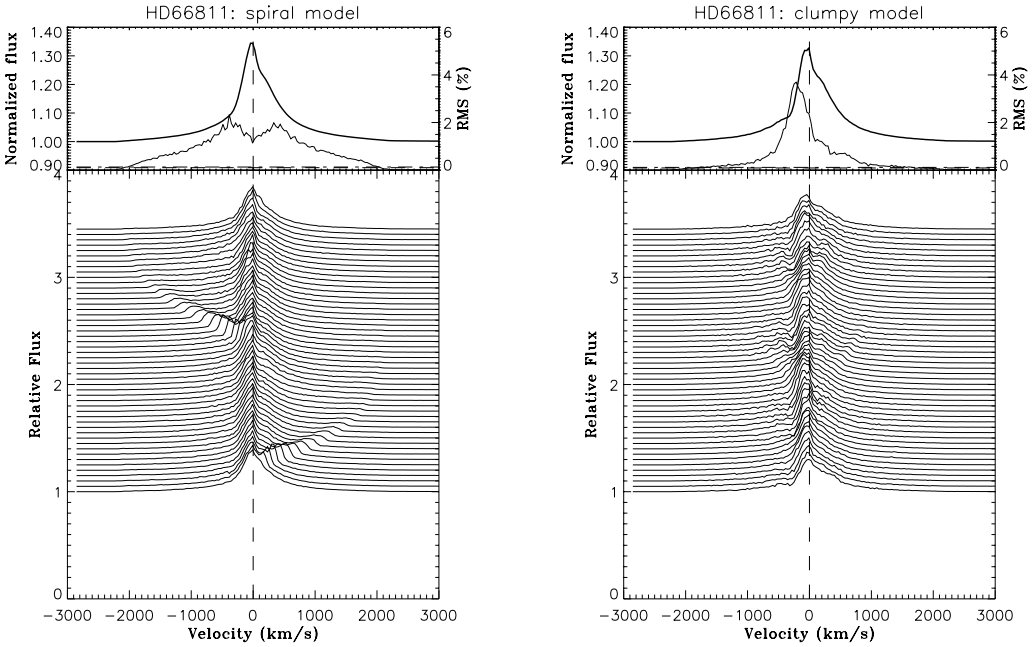

Fig. 10. As Fig. 1, however for the time-series of synthetic Hαprofiles from ζ Pup as calculated by Harries (2000), using two different 3-D models for the wind morphology. *Left panel*: wind with co-rotating, one-armed spiral density enhancement; *right panel*: clumped wind. Note the different distributions of the corresponding TVS.

from the 3-D simulations are free of noise, in contrast to the spectra from our 1-D models.

These findings suggest that at least in the case of a clumpy wind the TVS signatures do not or little depend on the specific model, and that the results of our simple 1-D simulations are comparable to those from more realistic simulations. A final conclusion concerning this point can be drawn only when a larger set of 3-D simulations for a variety of wind parameters are available.

From the point of view of the observations, on the other hand, the above finding means also that the probability of obtaining a symmetric TVS of Hαwill be very low if the wind is clumpy, even if using snapshot observations.

7. Spectral variability and the Wind Momentum Luminosity Relationship

The most extreme case of snapshot observations occurs when performing a spectral analysis, since usually only one spectrum (or two consecutive ones) is/are available. Because of the spectral variability inherent to the objects under discussion, these individual data might be not very representative. In the following, we shall investigate this point with respect to derived mass-loss rates, with special emphasis on the question of how far the Wind Momentum Luminosity Relationship (WLR) of Galactic O-type stars is influenced.

To this end we assume (i) that the observed variability of Hα is only due to processes in the wind (i.e., the contribution of absorption lpv is neglected) and (ii) that this variability is interpreted in terms of a variable mass-loss rate. Note that the latter assumption is inherent to a typical spectrum analysis, since due to the scarcity of the available data-set(s) a particular mass-loss rate is derived, which of course might be not representative.

Following this philosophy, we derived upper and lower limits of the mass-loss rate for all our sample stars, from the two most extreme spectra present in the time-series, and calculated the corresponding limits for the modified wind-momentum rate. Due to the adopted simplifications (standard model, no clumping) the obtained values of $\dot{M}$ might be overestimated.

The mass-loss rate estimates listed in Table 2 show that the observed variations in $\dot{M}$ range from ±4% of the mean value, for stars with stronger winds, to ±16% for stars with weaker winds. Since the accuracy of our determinations also depends on the strength of the wind - ±20%, for stars with Hα in emission, and ±30%, for stars with pure absorption profiles (Markova et al. 2004) - we conclude that the observed variability of $\dot{M}$ does not exceed the errors of individual determinations and thus is not significant. This result is surprising, especially in those cases when drastic changes in the Hα profile shape have been observed. Note, however, that for not too low wind densities small changes in $\dot{M}$ give rise to large changes both in the profile shape and in the *EW* (Puls et al. 1996).

The derived amplitudes of the $\dot{M}$ variability have been used to place constraints on the variability of the corresponding wind momentum rates. The results indicate that wind variability affects the momentum rates by less than 0.16 dex, which is smaller than the error of individual estimates (0.30 dex, Markova et al. 2004) and thus is insignificant. It can be seen from Fig. 11, the uncertainty caused by wind variability does not provide any clue to resolve the problem concerning the WLR of Galactic O-type stars being a function of luminosity class (Puls et al. 2003; Repolust et al. 2004; Markova et al. 2004).

The assumption of a homogeneous and spherically symmetric wind (underlying our analysis) is in contrast to the presence of large-scale perturbations in the winds of some of our

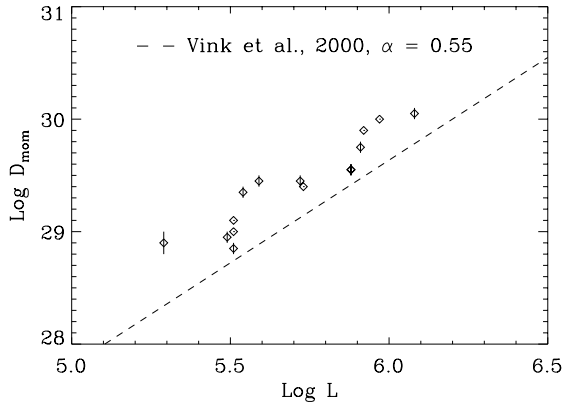

Fig. 11. WLR for our sample of Galactic O-type stars. Error bars display the influence of Hα lpv (interpreted in terms of $\dot{M}$) on the modified wind-momenta.

targets, which have been suggested by different investigators on various occasions (see Sect. 4). Consequently, problems may occur when trying to fit the Hα profiles with model calculations. For example, in HD 210 839, we failed to obtain a good fit for a number of profiles of the time series.

8. Summary, discussion and conclusions

Although line-profile variability of Hα in O-type supergiants has been known for a relatively long time (e.g., Rosendhal 1973; Conti & Frost 1977), our survey is the first where this variability is detected and quantified in an objective and statistically rigorous manner for a large sample of stars. By means of a comparative analysis we were able to place a number of constraints on the properties of this variability as a function of stellar and wind parameters.

The main results of our survey can be summarized as follows:

To study the wind variability in O supergiants, as traced by Hα, we employed the TVS analysis, originally developed by Fullerton et al. (1996), however modified to account for the effects of wind emission of various strength on the observed profiles. As already predicted by these authors, the so-called fractional amplitude of deviations, which serves as a measure for *absorption* lpv, cannot serve as an indicator for the strength of wind variability. Instead, we introduced and used a new TVS parameter, $a_{\rm N}$, which measures the contribution of unit wind emission to the variability detected by the corresponding TVS.

By means of this quantity we found that the observed variability of Hα per unit wind emission is a moderately decreasing function of mean wind density. This result might be interpreted as an indication that stronger winds are less active than weaker ones. However, at least on the basis of our present, simplistic line-profile simulations, this hypothesis cannot be supported.

All sample stars show evidence of *significant* line-profile variations in Hα with *mean* amplitudes $A_{\rm N}$ between 1 and 4% of the continuum strength. Since absorption lpv seems to be common among O-type stars (Fullerton et al. 1996), these amplitudes can in principle be due to a combination of variations generated both in the photosphere and in the wind. However, our analysis indicates that even at lower wind densities ($\log\langle\rho\rangle \approx -14$) contributions from wind effects have to be accounted for, and that for a number of stars wind variability is actually the dominating source.

In their original study, Fullerton et al. concluded that the mean amplitude of the deviations is an inappropriate quantity to compare lpv in different lines of various stars because it does not account for the strength of the underlying feature. Although true for the case of absorption lpv, this conclusion has to be somewhat modified with respect to our investigations. By means of simple line-profile simulations, the mean amplitude of deviations in Hα (defined by Eq. (10)) has been predicted to be an increasing function of mean wind density, at least in those cases where the disturbances in density were present everywhere in the wind. Interestingly, this prediction is *not* supported by our observations which gave no evidence of any correlation between mean amplitude and density. Moreover, a comparison of observed mean and fractional amplitude with corresponding simulated quantities gives different information, because of the different influence of either the contributing velocity range of *significant* variability or the contributing net wind emission. Both quantities (i.e., fractional *and* mean amplitude) deserve their own treatment and have to be reproduced simultaneously by future models which claim to explain the observed variability.

Fullerton et al. (1996) have found that the *distribution* of variability within an absorption profile can provide information about the cause of the variations, e.g., radial or non-radial pulsations. By means of a series of models with different wind morphology we showed that the TVS analysis of Hαcan also give some insight into the structure of the wind, at least of its lower part where this line forms. Both models with spherically symmetric and with broken shells produce an Hα TVS with a blue-to-red asymmetry, if the structures are distributed uniformly over the contributing wind volume and as long as the wind-density is not too large. The only difference in the outcome of the two kinds of models is the actual degree of the asymmetry: at the same mean density, shell models produce less asymmetry than those with broken shells (i.e., blobs). Moreover, this result does not seem to depend on whether snapshots or systematic simulations are used. Note, however, that an asymmetric large-scale, long-lived co-rotating structure will always produce a symmetric TVS *if* the whole period of rotation is covered by observations.

A comparison between the observations and line-profile simulations (assuming variations caused by coherent shells/blobs distributed everywhere in the wind) revealed that for stars of *intermediate* wind density the parameters of the Hα TVS are consistent with those from the models if one allows for a scatter within a factor of two for the maximum (relative) amplitude of the disturbances at given wind density.

On the other hand, the established disagreement at lower and higher wind densities might simply point to the presence of wind effects which are not accounted for in our simulations. For example, to reproduce the variations observed in Hα at lower wind densities one might suggest the presence of a radially extended, coherent structure in front of the disk which can mimic variations in the global mass-loss rate. The major problem

concerning the (two) stars with stronger winds relates to the fact that the observations yield a TVS which is localized preferentially bluewards of the rest frame (inside a rather narrow velocity range), whereas our simulations always produce an almost symmetric TVS instead. This discrepancy might be again interpreted in terms of a rather confined region of variability close to the star.

Our analysis shows that *significant* variations in Hα occur below 0.3 v_∞. This estimate is slightly higher than the value derived by Kaper et al. (1997), namely 0.2 v_∞. Since the velocity extent of the observed variations depends strongly on $\langle\rho\rangle$ and since our sample includes a few stars with strong winds (Hα completely in emission) which are missing in the sample of Kaper et al., such a discrepancy is quite natural. Moreover, the velocity limits as derived by us, converted to units of physical space, correspond to 1.4 to 1.5 $R_\star$, in good agreement with results from theoretical calculations with respect to the outer limits of Hα line-formation in O supergiant winds.

Interpreted in terms of variable mass-loss rates, the observed (partly extreme) variations in the Hα wind emission indicate variations in $\dot{M}$ of ±4% of the mean value for stars with stronger winds and of ± 16% for stars with weaker winds. The ratio of maximum to minimum mass-loss rate determined over the time interval present for our sample ranges from 1.08 to 1.47, with a tendency that weaker winds show larger values. The mean ratio averaged over the whole sample is 1.22, in good agreement with the value provided by Prinja & Howarth (1986).

The consequences of wind variability with respect to the wind momentum rate of the sample stars is smaller than 0.16 dex and hence not significant, given the individual errors inherent to any $\dot{M}$ determination. This result agrees well with the investigation by Kudritzki (1999) who reported 0.15 dex as the error in the wind momentum rate of one A-supergiant, HD 92 207, introduced by wind variability. Thus, we conclude that wind variability in O supergiants does not seem to affect the main concept of the WLR although it might contribute to the local scatter by moving individual points (up and down) with respect to each other.

The Hα profiles of the sample stars derived throughout our observations are quite similar, both in shape and strength, to those obtained by other investigators in various epochs (e.g., Rosendhal 1973; Conti & Frost 1977; Scuderi et al. 1992; Ebbets 1982; Underhill 1995; Kaper et al. 1997). This finding suggests that the atmospheres of our targets are not subject to long-term variability. On the other hand, no information about previous Hαobservations concerning the stars BD+56 739 and HD 338 926 was found in the literature.

Acknowledgements. We thank the referee. Dr. Alex Fullerton, for his valuable comments and suggestions which helped to improve the paper. We are also grateful to Dr. T. Harries for providing us with the data from his 3-D wind simulations. This work was supported in part by a NATO Collaborative Linkage Grant, (No. PST/CLG 980007) and by a National Scientific Foundation to the Bulgarian Ministry of Education and Science grant (No.1407).

References

Bianchi, L., & Garcia, M. 2002, ApJ, 581, 610
Conti, P. S., & Frost, S. A. 1977, ApJ, 212, 728
Crowther, P. A., Hillier, D. J., Evans, C. J., et al. 2002, ApJ, 579, 774
Dessart, L., & Owocki, S. P. 2003, A&A, 406, L1
Ebbets, D. 1982, ApJS, 48, 399
Feldmeier, A. 1995, A&A, 299, 523
Fullerton, A. W., Gies, D. R., & Bolton, C. T. 1992, ApJ, 390, 650
Fullerton, A. W., Gies, D. R., & Bolton, C. T. 1996, ApJS, 103, 475
Gies, D. R. 1987, ApJS, 64, 545
Groenewegen, M. A. T., & Lamers, H. J. G. L. M. 1989, A&AS, 79, 359
Hamann, W.-R. 1980, A&A, 84, 342
Harries, T. 2000, MNRAS, 315, 722
Herrero, A., Kudritzki, R.-P., Vilchez, J. M., et al. 1992, A&A, 261, 209
Israelian, G., Herrero, A., Musaev, F., et al. 2000, MNRAS, 316, 407
de Jong, J. A., Henrichs, H. F., Schrijvers, C., et al. 1999, A&A, 345, 172
de Jong, J. A., Henrichs, H. F., Kaper, L., et al. 2001, A&A, 368, 601
Kaper, L., Henrichs, H. F., Fullerton, A. W., et al. 1997, A&A, 327, 281
Kaper, L., Henrichs, H. F., Nichols, J. S., & Telting, J. H. 1999, A&A, 344, 231
Kaufer, A., Stahl, O., Wolf, B., et al. 1996, A&A, 305, 887
Kudritzki, R.-P. 1999, in Proc. IAU Coll. 169, ed. B. Wolf, O. Stahl, & A. W. Fullerton (Sprimger Verlag), 405
Kudritzki, R.-P., & Puls, J. 2000, ARA&A, 38, 613
Markova, N. 1986, A&A, 162, L3
Markova, N. 2002, A&A, 385, 479
Markova, N., & Valchev, T. 2000, A&A, 363, 995
Markova, N., Puls, J., Repolust, T., et al. 2004, A&A, 413, 693
Massa, D., Fullerton, A. W., Nichols, J. S., et al. 1995, ApJ, 452, L53
Meynet, G., Maeder, A., Schaller, G., et al. 1994, A&AS, 103, 97
Owocki, S. P., & Puls, J. 1999, ApJ, 510, 355
Owocki, S. P., Castor, J. I., & Rybicki, G. B. 1988, ApJ, 335, 914
Press, W. H., Flannery, B. P., Teukolsky, S. A., et al. 1992, Numerical Recipes: The Art of Scientific Computing, 2nd edition (Cambridge: Cambridge Univ. Press), 634f
Prinja, R. K., & Howarth, I. D. 1986, ApJS, 61, 357
Prinja, R. K., & Smith, L. J. 1992, A&A, 266, 377
Prinja, R. K., & Fullerton, A. 1994, ApJ, 426, 345
Prinja, R. K., Balona, L. A., Bolton, C. T., et al. 1992, ApJ, 390, 266
Prinja, R. K., Fullerton, A. W., & Crowther, P. A. 1996, A&A, 311, 264
Prinja, R. K., Stahl, O., Kaufer, A., et al. 2001, A&A, 367, 891
Prinja, R. K., Massa, D., & Fullerton, A. W. 2002, A&A, 388, 587
Puls, J., Kudritzki, R.-P., Herrero, A., et al. 1996, A&A, 305, 171
Puls, J., Repolust, T., Hoffmann, T., et al. 2002, in Proc. IAU Symp. 212, ed. K. A. van der Hucht, A. Herrero, & C. Esteban, ASP Conf. Ser., 61
Rauw, G., Morrison, N. D., Vreux, J.-M., et al. 2001, A&A, 366, 585
Repolust, T., Puls, J., & Herrero, A. 2004, A&A, 415, 349
Rosendhal, J. F. 1973, ApJ 186, 909
Scuderi, S., Bonanno, G., Di Benedetto, R., et al. 1992, ApJ, 392, 201
Underhill, A. B. 1995, ApJS, 100, 433
Vink, J. S., de Koter, A., & Lamers, H. J. G. L. M. 2000, A&A, 362, 295
Walborn, N. R. 1973, AJ, 78, 1067